Coupling Mineralogy, Textures, Stable and Radiogenic Isotopes in Identifying Ore-Forming Processes in Irish-Type Carbonate-Hosted Zn–Pb Deposits

**Lola Yesares [1,*], Drew A. Drummond [2], Steven P. Hollis [1,3] , Aileen L. Doran [1] ,
Julian F. Menuge [1] , Adrian J. Boyce [2], Robert J. Blakeman [4] and John H. Ashton [4]**

[1] iCRAG and School of Earth Sciences, University College Dublin, Belfield, 4 Dublin, Ireland;
steve.hollis@icrag-centre.org (S.P.H.); aileen.doran@icrag-centre.org (A.L.D.); j.f.menuge@ucd.ie (J.F.M.)

[2] Scottish Universities Environmental Research Centre, East Kilbride, Glasgow G75 0QF, UK;
drewdrummond59@gmail.com (D.A.D.); adrian.boyce@glasgow.ac.uk (A.J.B.)

[3] Geological Survey Ireland, Beggars Bush, 4 Dublin, Ireland

[4] Boliden Tara Mines DAC, Navan, Co. Meath, Navan, Ireland; Robert.Blakeman@boliden.com (R.J.B.);
John.Ashton@boliden.com (J.H.A.)

* Correspondence: lola.yesares@icrag-centre.org; Tel.: +353-1-716-2331

Abstract: Irish-type deposits comprise carbonate-hosted sphalerite- and galena-rich lenses concentrated near normal faults. We present new data from the Tara Deep resource and overlying mineralization, at Navan, and the Island Pod deposit and associated Main zone orebodies, at Lisheen. Tara Deep mineralization predominantly replaces Tournasian micrites and subordinate Visean sedimentary breccias. The mineralization is mainly composed of sphalerite, galena, marcasite and pyrite. A range of Cu- and Sb-bearing minerals occur as minor phases. At Tara Deep, paragenetically early sulfides exhibit negative $\delta^{34}S$ values, with later phases displaying positive $\delta^{34}S$ values, indicating both bacterial sulfate reduction (BSR) and hydrothermal sulfur sources, respectively. However, maximum $\delta^{34}S$ values are heavier (25‰) than in the Main Navan orebody (17‰). These mineralogical and isotopic features suggest that Tara Deep represents near-feeder mineralization relative to the Navan Main orebody. The subeconomic mineralization hosted in the overlying Thin Bedded Unit (TBU) comprises sphalerite replacing framboidal pyrite, both exhibiting negative $\delta^{34}S$ values (−37.4 to −8.3‰). These features indicate a BSR source of sulfur for TBU mineralization, which may represent seafloor exhalation of mineralizing fluids that formed the Tara Deep orebody. The Island Pod orebody, at Lisheen, shows a mineralogical paragenetic sequence and $\delta^{34}S$ values broadly similar to other Lisheen orebodies. However, the lack of minor Cu, Ni, and Sb minerals suggests a setting more distal to hydrothermal metal feeder zones than the other Lisheen orebodies. Pb isotope data indicate a very homogeneous Lower Palaeozoic Pb source for all Navan orebodies. Lower Palaeozoic metal sources are also inferred for Lisheen, but with variations both within and between orebodies. Carbon and oxygen isotopic variations at Navan and Lisheen appear to result from fluid-carbonate rock buffering. The emerging spectrum of mineralogical and isotopic variations define proximal to distal characteristics of Irish-type systems and will assist in developing geochemical vectoring tools for exploration.

Keywords: carbonate-hosted; Zn–Pb; S isotopes; mineralogy; C–O isotopes; Irish-type

1. Introduction

Irish-type Zn–Pb deposits consist primarily of stratabound sphalerite, galena, and iron sulfides, accompanied by dolomite, calcite and barite as gangue, hosted in carbonate sedimentary rocks. They are concentrated near normal faults, which are often associated with the development of Upper Palaeozoic sedimentary basins [1]. Economic deposits of this type were first recognized through the discovery of the Tynagh deposit in Co. Galway during the early 1960s [2]. Later, further deposits were discovered, for example the Navan, Lisheen, Silvermines, Galmoy, and Pallas Green deposits.

As metallogenetic understanding of the Irish Midlands developed, it became clear that these deposits, although sharing similar characteristics with Mississippi Valley-type (MVT) and sedimentary exhalative (SEDEX) deposits, are distinct in several key aspects. Irish-type deposits formed primarily by carbonate replacement, like MVT deposits, and only occasionally show characteristics of exhalative mineralization [3]. Carbonate replacement is typically stratabound and took place early in the diagenetic history of the host rocks; and although primarily epigenetic, the process of ore formation was intimately connected with sedimentation and extensional tectonics, similar to SEDEX models. Consequently, these deposits are regarded as hybrids between MVT and SEDEX styles of mineralization. The term Irish-type came into informal use in the 1980s but is now used to classify deposits world-wide. These include carbonate-hosted deposits in the Cambrian of the Kootenay Arc, British Colombia, Canada; the Neoproterozoic of the Vazante Group, Minas Gerais, Brazil [4]; and the Cretaceous of Iran [5].

Early work on Irish-type deposits stressed the exhalative aspects of their origin, supported by unequivocal evidence from the Silvermines and Navan deposits [6–8] but also referencing the colloform and other banded sulfide ore textures that are common in these deposits. However, increasing petrographic evidence led to a change in understanding during the 1990s. For example, in the Navan and Lisheen deposits, ore sulfides have replaced host carbonates and associated bioclasts [9,10]. The banded ore, common to most Irish Zn–Pb deposits, is now regarded as the result of sulfide crystallization accompanying carbonate host rock dissolution, with colloform textures forming in dissolution cavities [11,12].

The Navan deposit is a world-class carbonate-hosted Zn–Pb deposit mined by Boliden Tara Mines and supports Europe's largest zinc mine. Following an extensive seismic survey in 2012 [13], a new satellite orebody to the Navan deposit was discovered, known as Tara Deep, with an inferred resource of 18.2 Mt at 7.6% Zn and 1.6% Pb [14]. The total mined tonnage and in-situ resources at Boliden Tara Mines at the of end 2018 comprised 135.7 Mt grading 7.7% Zn and 1.8% Pb, including Tara Deep [14]. The orebody is hosted by Tournasian limestones and is located in the northern margin of the Dublin Basin (Figure 1). Comprehensive studies of the Navan deposit are mostly based on structural, petrologic and geochemical analyses of both the Main Orebody and South West Extension (SWEX) [6,7,9,15–19]. However, the newly discovered Tara Deep Orebody is still poorly understood [13].

The Lisheen deposit had initial resources of 16.7 Mt at 14.1% Zn and 2.4% Pb [20], with the relatively recently discovered Island Pod having an additional inferred resource of 0.3 Mt at 20% Zn and 1.6% Pb. Lisheen was mined by Vedanta Resources until late 2015. The deposit is associated with hydrothermal dolomite forming the matrix of brecciated bodies hosted by the Tournasian Limestone and is located on the Rathdowney Trend [10] (Figure 1). Numerous workers address the main geological features at Lisheen, such as stratigraphy, structure, petrology and geochemistry [10,12,20–25] but the Island Pod orebody is less well understood due to its recent discovery.

Here, we focus on the mineralogy of two recently discovered deposits in the Irish orefield, Tara Deep at Navan, and the Island Pod at Lisheen, and their geochemical halos. These observations are coupled with new S isotope analyses, Pb isotope compositions, and carbonate C and O analyses, to elucidate variations within large hydrothermal systems in the Irish Midlands. This research will contribute to our understanding of the principal mechanisms of ore genesis of carbonate-hosted deposit globally.

2. Geological Setting

The Irish Midlands are dominated by Lower Carboniferous limestones (Figure 1). These rocks were deposited in tropical, typically shallow, seas and associated with sedimentary basins developed during crustal extension [26]. They represent a marine transgression over clastic sedimentary rocks of late Devonian to Tournasian age known as the Old Red Sandstone, a terrestrial/littoral red bed succession [26]. Irish-type deposits are developed primarily in Tournasian carbonate sedimentary rocks at two distinct stratigraphic levels. The Navan deposit, and some smaller deposits in the northeastern Irish Midlands, are hosted mainly by micrites in the basal Tournasian limestone sequence [11]. Further to the south and west, deposits including Lisheen, Galmoy and Silvermines are hosted in dolomitized Waulsortian limestones. In both cases, these consist of the stratigraphically oldest limestones in their respective regions [27].
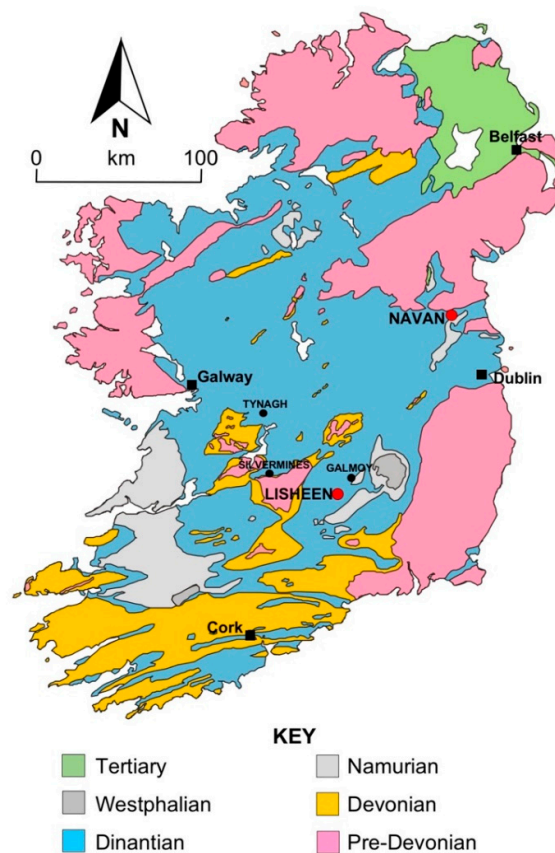
Figure 1. Simplified geological map of Ireland including the location of the Navan and Lisheen deposits (Modified from Gagnevin et al. [28]).

The Old Red Sandstone of the Irish Midlands was deposited on an eroded basement of Ordovician to Silurian metasedimentary and metavolcanic rocks. These rocks were brought together, deformed and metamorphosed by the closure of the Iapetus ocean during the Caledonian orogeny [2,3]. They are in most places covered by Devonian and younger rocks and consequently poorly understood. In the southeast Midlands they were probably deposited on the microcontinent of Ganderia–Avalonia [29]. Combined seismic and lower crustal xenolith studies suggest that Precambrian crust may be absent beneath the Iapetus suture zone [30], which underlies much of the Irish Midlands.

The mineralogy and fine-grained textures of Irish-type deposits have proved a major obstacle to most isotopic dating attempts. Ages based on remnant magnetism [31–34] are contentious because of conflict with geological constraints. However, recent palaeomagnetic analyses of rocks distal to mineralization have yielded similar remnant magnetic directions to mineralized rocks; the ~310 Ma

apparent polar wander path age is consistent with a magnetization event during the Variscan orogeny [31,32]. Consequently, ages based on palaeomagnetic data are probably unrelated to ore formation. Ore-stage pyrite from Lisheen has yielded a well constrained Re-Os isochron age of 346.6 ± 3 Ma, whilst a slightly less secure errorchron (MSWD = 19) age of 334.0 ± 6.1 Ma was obtained from Silvermines pyrite [35]. Observations of sulfide clasts in a Lower Visean conglomerate at Navan suggest that at least some mineralization here is of Lower Visean age [11], consistent with the Lisheen Re–Os date.

3. Samples and Methods

Samples from Tara Deep and Lisheen, that encompass many of the varied mineralization styles and host rocks, were collected from drill cores extracted by Boliden Tara Mines and Vedanta Resources Ltd., respectively. The mineralogical, textural, and paragenetic analyses were carried out by transmitted and reflected light microscopy and Scanning Electron Microscopy-Energy Dispersive Spectroscopy (SEM-EDS) at University College Dublin (Dublin, Ireland), the University of Glasgow (Glasgow, UK), the University of Huelva (Huelva, Spain) and Memorial University Newfoundland (St. John's, NL, Canada).

Sulfur isotope analyses were carried out on representative sulfides from the Tara Deep orebody and the overlying Thin Bedded Unit at Navan, and the Island Pod and the Main zone at Lisheen. In-situ laser ablation analyses of sulfide $\delta^{34}S$ in polished sections, selected on the basis of the petrological study, were made using the established technique described by Kelley and Fallick [36] at the Scottish Universities Environmental Research Centre (SUERC). The polished sections were inserted into a sample chamber which was evacuated and subsequently filled with an excess of oxygen gas. A spot (~300 microns in diameter) of the sulfide was combusted using a Spectron Lasers 902QCWNd:YAGlaser (1W power). The released SO_2 gas was purified in a vacuum line. Determination of the sulfur isotope composition of the purified SO_2 gas ($\delta^{66}SO_2$) was carried out using a VG SIRA II gas mass spectrometer. All sulfur isotope compositions were calculated relative to Cañon Diablo Troilite (CDT), and are reported in standard notation. Reproducibility based on complete duplicate analyses (including combustion) was better than 0.3 per mil. Experimentally determined sulfide mineral fractionation corrections for the SUERC laser and gas line system were calibrated for all base metal sulfides analyzed.

Carbonate isotope measurements ($\delta^{13}C$ and $\delta^{18}O$) of calcite and dolomite phases were obtained from both the Lisheen and Navan deposits [37,38]. Carbonate phases were characterized by traditional petrography and Scanning Electron Microscopy at University College Dublin, and imaged using a CITL mk5 cold cathode-luminescence stage mounted on a Nikon 50i microscope at Imperial College London (London, UK). Sample powders were obtained using a handheld rotary drill. Clumped C–O isotope analysis was performed at the University of East Anglia (Norwich, UK). Carbon dioxide was produced by reacting 3–5 mg of carbonate powder with orthophosphoric acid in vacuo at 25 °C for a period of 12 h for calcite and 5 days for dolomite. Subsequent samples were reacted at a temperature of 90 °C for 20 min. The evolved CO_2 was collected by cryo-distillation according to the methodology outlined by Dennis et al. [39]. Sample gases were analyzed for their isotope values on a custom-built MIRA (multiple isotope ratio analyzer) dual-inlet mass spectrometer [39]. The external precision for sample analysis is estimated as ±0.014‰.

Pb isotope analyses were carried out on representative galenas extracted using a handheld drill from Tara Deep, the Main Orebody and from Tatestown in the Navan area, and from all of the ore lenses at Lisheen. Approximately 5 mg of galena was dissolved by adding 2.5 mL of 6 mol/L HCl and 250 μL of 70% HNO_3. The samples were dried down on a hotplate at ~120 °C, and re-dissolved in 19 mL of deionized water and 1mL of 70% HNO_3. Subsequently, an aliquot of 10 μL was taken, centrifuged, diluted with 2.5 mL of 3% HNO_3, and spiked with 25 μL of thallium solution of known $^{203}Tl/^{205}Tl$ ratio to correct for mass bias fractionation. Sample solutions were analyzed using a Thermo-Scientific Neptune multi-collector inductively coupled plasma mass spectrometer at the National Centre for Isotope Geochemistry, University College Dublin (UCD). The two year mean values of standard

NIST NBS 981 (*n* = 36) for this method at UCD are $^{206}Pb/^{204}Pb$ = 16.9350, $^{207}Pb/^{204}Pb$ = 15.4896 and $^{208}Pb/^{204}Pb$ = 36.6920. Data was corrected to the recommended Pb isotopic ratios for NIST NBS 981 of Yuan et al. [40]. The two year standard deviation of NBS 981 for this method at UCD are $^{206}Pb/^{204}Pb$ = 0.0038%, $^{207}Pb/^{204}Pb$ = 0.0049% and $^{208}Pb/^{204}Pb$ = 0.0073%.

4. Geology of the Deposits

4.1. The Navan Deposit and Tara Deep Orebody

The Tara Deep orebody is located ~3 km SE of the South West Extension (SWEX) of the Navan deposit, at a depth of 1.2–1.9 km (Figure 2a). Tara Deep consists of a Zn–Pb semi-massive sulfide body, up to 60 m thick.

In the Navan area, the stratigraphic succession comprises the Tournasian basal limestone sequence, which forms the Navan Group, overlain by the Visean marine succession comprising the Fingal Group. The Navan Group consists of the footwall sequence of Red Beds, Laminated Beds, and Muddy Limestone (Figure 2b). These shallow water units, as well as the overlying Pale Beds, form allochthonous slide blocks which in turn are overlain by melange-like deposits of Shaley Pales, and/or Argillaceous Bioclastic Limestones. This allochthonous package is overlain by the Fingal Group, which comprises lenses of polymict submarine debris-flows overlain by a deep marine succession of interbedded, distal calc-turbidites, and shales known as the Upper Dark Limestone (UDL) (Figure 2b).
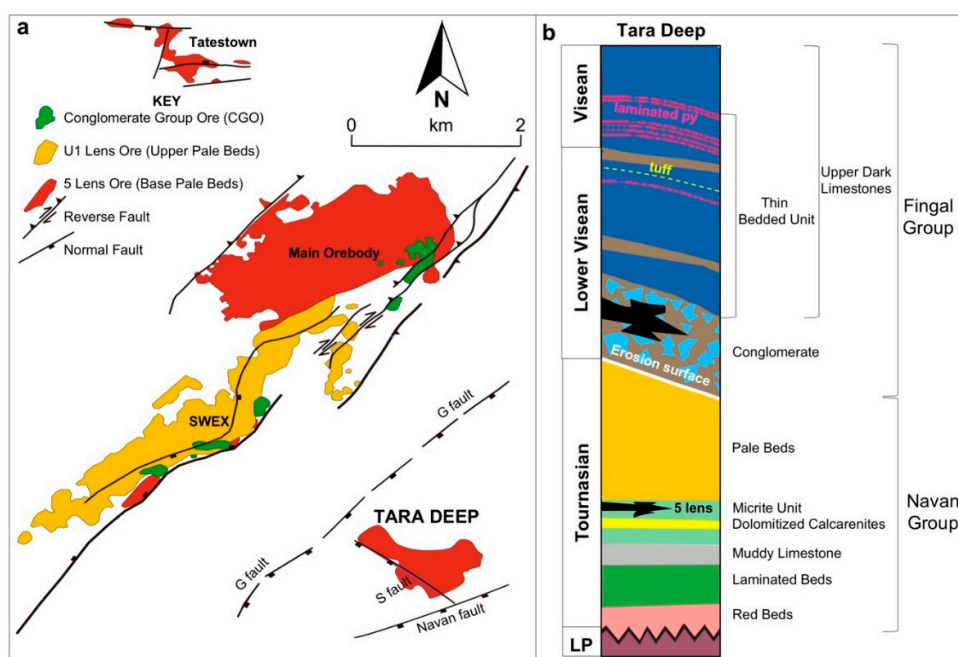
Figure 2. Geology of the Navan orebody including the Tara Deep deposit (**a**) Map projection of the top surface of the Navan system, including the different deposits and main structural features (modified from Ashton et al. [11]); (**b**) Stratigraphic column of the Tara Deep area showing the different ore lenses and hosting rocks. (L.P. = Lower Palaeozoic).

Tara Deep is located between two major extensional structures. The G Fault forms the northern boundary, while the southern limit is defined by a larger structure, the ENE-trending Navan Fault, which has a displacement of several kilometers. The structural terrace formed by the Navan and G faults is cut by the S fault, a NNW-striking, steep westerly dipping structure (Figure 2a).

Tara Deep shows similar mineralogical compositions and textural relationships to the Navan Main Orebody and SWEX [11], comprising sphalerite and galena (5:1 ratio), with minor pyrite, marcasite, barite, stibnite, and chalcopyrite.

At Tara Deep, mineralization occurs chiefly in two principal lithologies:

1. The Micrite Unit is the most important host, containing approximately 90% of the total resource [13], with stratabound mineralization occurring in fault-bounded blocks. Associated with a quiescent, sabkha-like depositional environment, the upper and lower micrites with an intervening calcitite can vary in thickness but are typically 50–60 m thick. Characteristic features include fine-grained, organic matter-rich, blue/dark grey, and abundant bird's-eye (fenestral) textures. The lower Micrite Unit is the most strongly mineralized and includes high-grade mineralization comprising replacive, massive sphalerite, galena, and marcasite (Figure 3a). The upper Micrite Unit shows variable but lower grades. For example, fracture-infilling mineralization is typically observed as a series of sulfide veins (Figure 3b). Commonly the micrites host alternating layers of sphalerite and galena (Figure 3c).

2. Sedimentary breccias located near the hanging walls of the G and S faults, towards the NW of Tara Deep, host the remainder of the mineralization. The sedimentary breccias are composed chiefly of Pale Beds clasts with minor Waulsortian Limestone, replaced and cemented by sulfide (Figure 3d,e). As in the Navan deposit, the sedimentary breccias also contain detrital sulfide clasts, again suggesting a Lower Visean age for at least some of the mineralization.
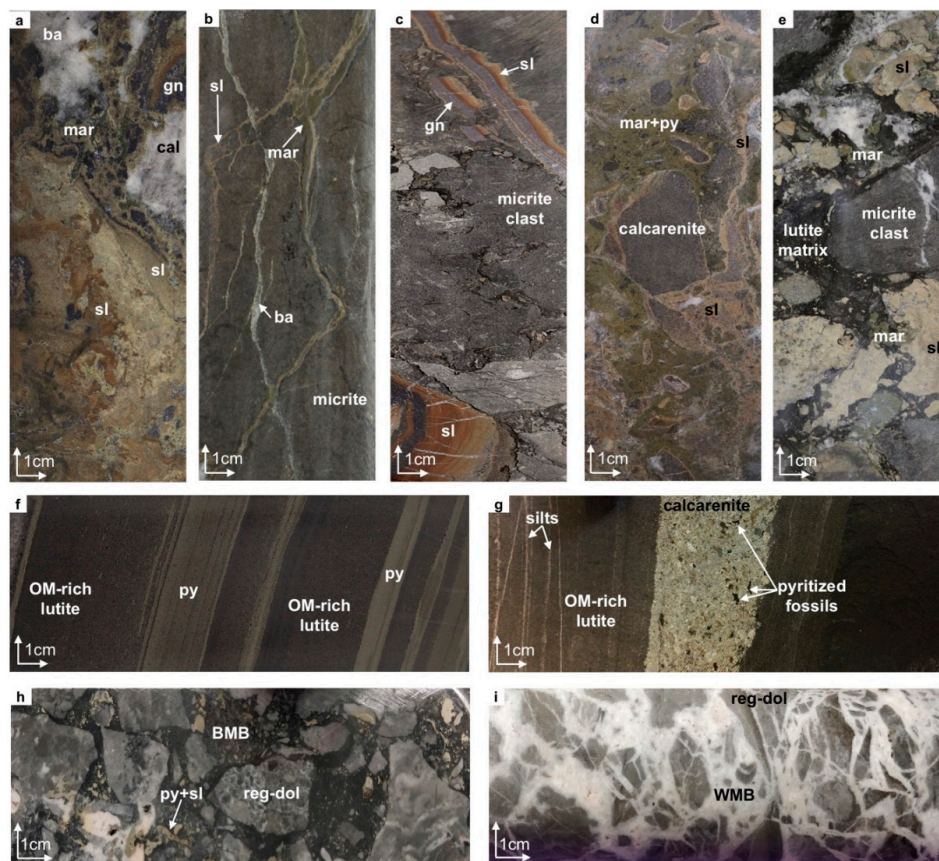
Figure 3. Main host facies and mineralization styles at Tara Deep (**a**–**e**), in the Upper Dark Limestone overlying Tara Deep (**f**,**g**) and breccia types at Lisheen (**h**,**i**). (**a**) High grade mineralization comprising massive sphalerite (sl), galena (gn) and marcasite (mar) with late barite (ba) and calcite (cal), replacing the host micrite; (**b**) low grade mineralization displaying marcasite, barite and sphalerite veining; (**c**) low grade mineralization formed by reworked micrite partially replaced by alternating layers of sphalerite and galena; (**d**) mineralized conglomerate comprising micrite clasts with sphalerite, marcasite, and pyrite (py) filling open spaces; (**e**) brecciated sphalerite mineralization hosted within disrupted Pale Beds-rich conglomerates; (**f**) organic matter-rich lutite replaced by ~0.5 to 1.5 cm layers of fine-grained pyrite parallel to bedding; (**g**) alternating sequences of organic matter-rich lutites, silts and calcarenites

including pyritized fossils; (**h**) black matrix breccia (BMB) comprising angular clasts of regional dolomite (reg-dol) cemented by sulfide-rich, fine-grained black dolomite; (**i**) white matrix breccia (WMB) from the Island Pod ore body comprising angular clasts of dolomitic Waulsortian limestone (regional dolomite) cemented by hydrothermal white, coarse-grained dolomite (dol).

The Tara Deep deposit is unconformably overlain by a deep marine succession, comprising the Visean basin fill, known as the Upper Dark Limestone (UDL) (Figure 2b). In the Tara Deep area, the lower UDL includes the Thin Bedded Unit (TBU), which comprises alternating sequences of dark lutites, siltstones, and bioclastic rocks (Figures 2b and 3f,g). Here, uneconomic seafloor sulfide mineralization has been identified above the Tara Deep deposit. It comprises 0.5–15 cm thick bedding-parallel layers of framboidal pyrite and minor disseminated sphalerite (Figure 3f). Mineralization is found extensively throughout the TBU, progressively increasing in abundance downwards. In addition, bioclastic layers within the TBU show a high degree of pyritization, including the replacement of fossils (Figure 3g).

4.2. The Lisheen Deposit and the Island Pod Orebody

The Lisheen deposit is composed of six separate stratabound orebodies, controlled by a network of normal faults: Main zone, Derryville, Bog Zone East, Bog Zone West, Bog Zone Central, and the Island Pod (Figure 4a). The Lisheen deposit is located in the hanging walls of extensional faults. They form a series of left-stepping, northerly dipping, en echelon structures (Figure 4a) that exhibit a classic ramp-relay geometry [3,25]. Locally, orebodies are controlled by a complex system of relaying listric faults associated with hydrothermal breccia development [25].

Several phases of dolomitization occur in the Lisheen area [41]. The earliest is a fine- to medium-grained, subhedral to euhedral grey dolomite that preferentially replaces micritic Waulsortian Limestone (D_{1a}) [42]. The latest consists of recrystallized coarse white dolomite (D_{1b}) that replaces coarser Waulsortian calcite crystals. Both dolomitization phases have been called the "regional dolomite" [42]. In the Lisheen deposit, the "regional dolomite" occurs in the footwalls of the main faults [43]. Mineralization at Lisheen is apparently related to a later hydrothermal dolomitization event towards the base of the Waulsortian limestones. This resulted in two main ore-related dolomites, which together with the sulfides, form the matrix of hydrothermal breccias and overprint the regional dolomite [10,24]: (1) The Black Matrix Breccia dolomite (D_2-BMB), is host to most of the economic mineralization and occurs as a fine-grained, black dolomite that replaces and infills open spaces in dolomitized Waulsortian limestone (Figures 3h and 4b); (2) the White Matrix Breccia dolomite (D_3-WMB) occurs as a coarse-grained white dolomite filling open spaces in dolomitized Waulsortian limestone (Figure 3i) and is developed above the BMB lenses within the Waulsortian (Figure 4b).

At Lisheen, mineralization occurs as stratabound, massive sulfide lenses within the base of the BMB, and as semi-massive sulfides in the Lisduff Oolite associated with both the footwalls and hanging walls of the major faults (Figure 4a). It mostly comprises pyrite, sphalerite, and galena. In addition, niccolite, tennantite, marcasite and chalcopyrite have been identified in close association to the feeder faults [20,24].
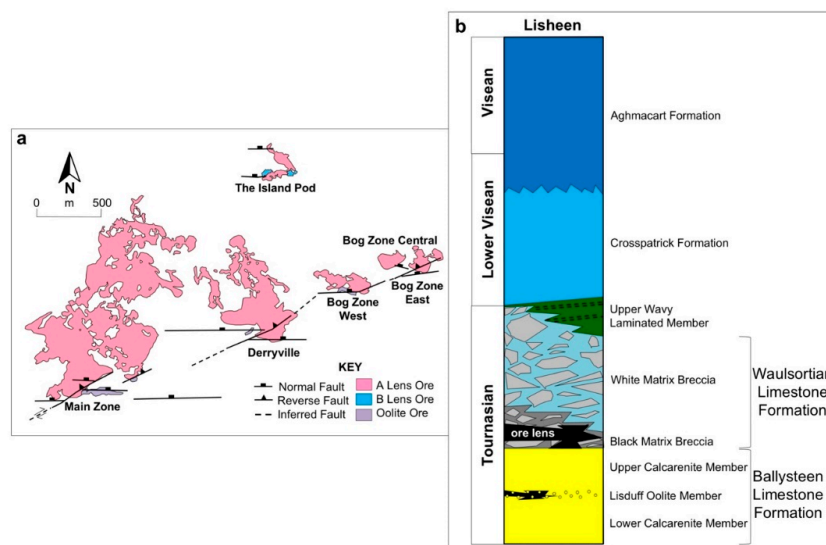
Figure 4. Geology of the Lisheen deposit. (**a**) Map projection of the top surface of the Lisheen deposit, including the different orebodies and main structural features (modified from Kyne et al. [44]). (**b**) Stratigraphic column of the Lisheen area showing the ore lens and hosting rocks (modified from Wilkinson et al. [45]).

5. Ore Mineralogy

5.1. Tara Deep, Navan

The main mineralogy of the Tara Deep deposit is similar to other deposits in the Navan system [11], but with minor mineralogical differences. Mineralization consists of sphalerite, galena, marcasite and pyrite, while stibnite, tetrahedrite, and chalcopyrite are minor components (Figure 5).

Pyrite is extensively distributed in the deposit, in both the Pale Beds and conglomerate-hosted mineralization. Pyrite shows a wide range of textures, including: Framboids, colloforms, recrystallized crystals, veinlets and fine-scale replacement of fossils. Two main pyrite generations have been recognized at Tara Deep. The first generation consists of framboidal pyrite partially replaced by colloform textures (Figure 5a) and fine-scale replacement of fossils (Figure 5b). It occurs as scarce relicts unevenly dispersed throughout the deposit. The second generation of pyrite is a recrystallization (Figure 5l) and replacement of marcasite aggregates (Figure 5j). It occurs dominantly throughout the mineralized breccias and conglomerates (Figure 3d,e).

Sphalerite is the dominant sulfide mineral in Tara Deep in both the Pale Beds and conglomerate-hosted mineralization. Sphalerite appears as filling interstices, replacements, veinlets, colloforms, and euhedral aggregates. Petrographic observations reveal two generations of sphalerite. Early sphalerite appears filling open spaces in earlier dolomite (Figure 5c), replacing early framboidal and colloform pyrite (Figure 5a,f), colloform sphalerite associated with dolomite (Figure 5d) and as fine euhedral aggregates (Figure 5e). A second generation of sphalerite has been identified as late infillings (Figure 5h), mostly in the mineralized breccias and conglomerates (Figure 3d,e).

Galena occurs in both the Pale Beds and conglomerate-hosted mineralization, and always shows a close relationship with sphalerite. It occurs mainly as skeletal aggregates, filling interstices and as euhedral coarse crystals. Two galena generations have been identified. The oldest generation appears mainly replacing primary pyrite textures (Figure 5a) and as skeletal aggregates embedded in colloform pyrite (Figure 5g). The younger generation occurs as a late infilling in pyrite and as coarse crystals associated with the second generation of sphalerite (Figure 5h). This galena generation contains inclusions of fine stibnite and tetrahedrite (Figure 5i).

Marcasite is widely distributed throughout the deposit but is most abundant within the calcarenites overlying the micrite horizons, and in the mineralized breccias and conglomerates (Figure 3b–e).

Marcasite occurs as veinlets, radial aggregates and with colloform texture. It is commonly observed partially replaced by the youngest pyrite generation (Figure 5j) and is also associated with the second sphalerite and galena generations.

Stibnite is a minor but common component of the Tara Deep deposit. It occurs in the second generation of coarse galena crystals, as very fine inclusions associated with tetrahedrite (Figure 5i) and as laths associated with the second generation of sphalerite (Figure 5k).

Chalcopyrite also appears in small amounts in the mineralized breccias and conglomerates. It is usually intergrown with the youngest sphalerite generation and filling interstices in pyrite aggregates (Figure 5l).
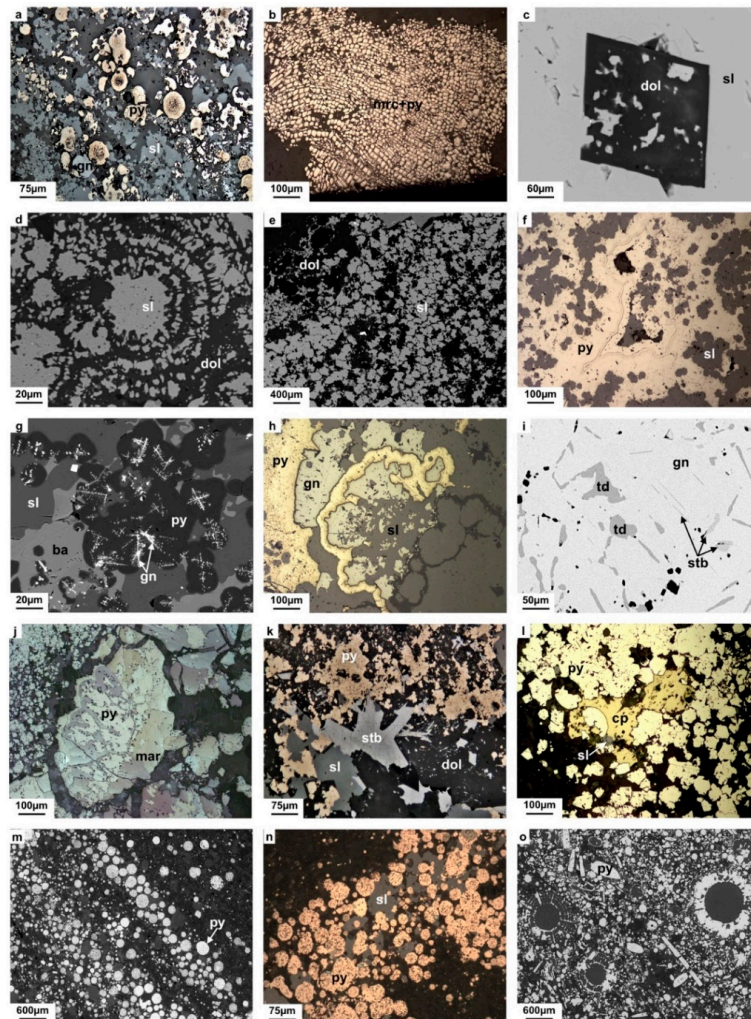
Figure 5. Reflected light and backscattered electron (BSE) images of the Tara Deep deposit (**a**–**l**) and the overlying UDL-hosted geochemical halo (**m**–**o**). (**a**) Relicts of framboidal pyrite (py) partially replaced by colloform pyrite and associated with sphalerite (sl) and galena (gn); (**b**) marcasite (mrc) and pyrite replacing wood cells; (**c**) euhedral dolomite (dol) crystal partially infilled and replaced by sphalerite; (**d**) dolomite replaced by colloform sphalerite; (**e**) subhedral sphalerite aggregates associated with dolomite; (**f**) sphalerite filling open spaces in colloform pyrite; (**g**) skeletal galena included in colloform pyrite; (**h**) interstitial galena and sphalerite in colloform pyrite; (**i**) fine tetrahedrite (td) and stibnite (stb) inclusions in galena; (**j**) marcasite partially corroded, replaced and overgrown by pyrite; (**k**) stibnite aggregates intergrown with sphalerite; (**l**) interstitial chalcopyrite (cp) in recrystallized pyrite; (**m**) laminated framboidal pyrite hosted in lutites; (**n**) laminated framboidal pyrite replaced by sphalerite; and (**o**) pyritized fossils (mainly radiolaria) in a calcarenite layer.

5.2. TBU Overlying Tara Deep, Navan

Pyrite and sphalerite comprise the main sulfide mineralogy of the uneconomic mineralization hosted in the overlying TBU at Tara Deep. Pyrite typically occurs as framboids forming 0.5–15 cm thick bedding-parallel layers which replace black mudstones (Figure 3f). These framboids have a very high degree of preservation (Figure 5m), with recrystallization being poorly developed. Pyrite also appears as a microfossil replacement, mainly of radiolaria (Figures 3g and 5o). Sphalerite occurs interstitially to, and replacing, pyrite framboids (Figure 5n).

5.3. Island Pod and Main Zone, Lisheen

Based on petrographic analysis of the Island Pod and Main zone orebodies, Lisheen mineralization consists mainly of pyrite, sphalerite, galena, and marcasite (Figure 6). Minor chalcopyrite, arsenopyrite, tennantite, cobaltite, gersdorffite, jordanite, bournonite, boulangerite, ullmannite, tetrahedrite, bravoite, pararammelsbergite, and niccolite have been reported from the Main zone, Derryville, and Bog zones [10,12,20,45].
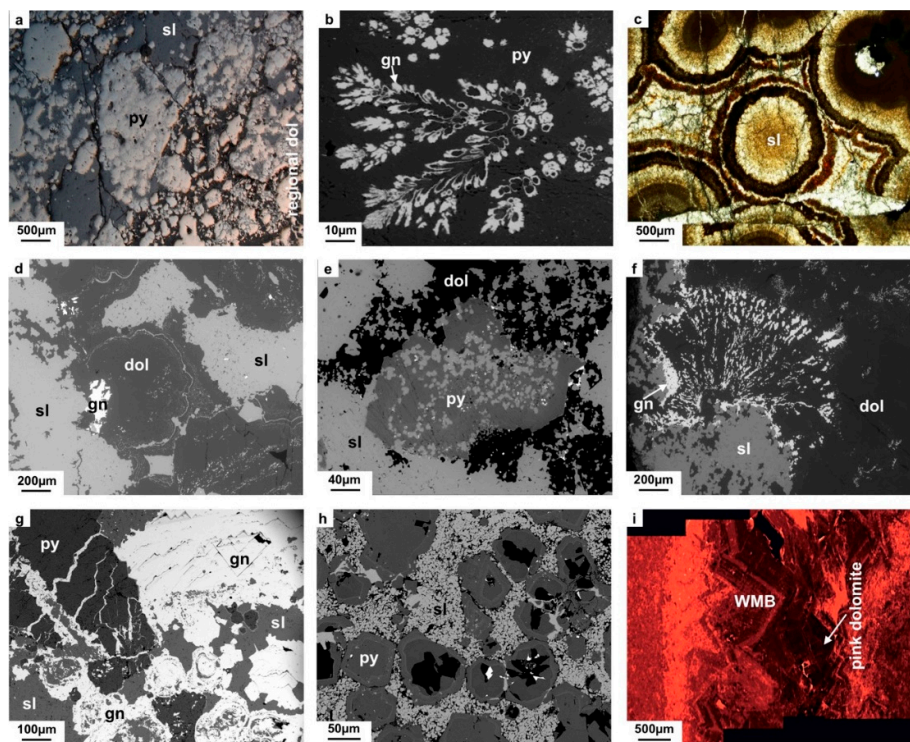
Figure 6. Reflected light, BSE and cathodoluminescence (CL) images of Lisheen deposit mineralization. (**a**) Relicts of primary pyrite (py) partially replaced by sphalerite (sl), Island Pod orebody; (**b**) dendritic pyrite (py) partially replaced by galena (gn), Island Pod orebody (modified from Doran et al. [46]); (**c**) colloform sphalerite, Derryville orebody; (**d**) intergrowth of sphalerite and dolomite (dol) on skeletal galena, Island Pod orebody (modified from Doran et al. [44]); (**e**) sphalerite replacing and filling interstices in pyrite, Island Pod orebody; (**f**) dendritic galena associated with dolomite and sphalerite, Island Pod orebody; (**g**) galena filling fractures in pyrite and replacing sphalerite, Main zone orebody; (**h**) zoned pyrite grain showing Co-As rims, with fracture infilling by sphalerite, Island Pod orebody; and (**i**) earlier regional dolomite overgrown by WMB dolomite and later infilling pink dolomite, Island Pod orebody.

Pyrite is extensively distributed in all the orebodies at Lisheen. It occurs in a variety of forms, often in close association with sphalerite and galena. Marcasite is relatively rare by comparison and is common near E–W normal faults and feeder zones. Several pyrite generations and morphologies have been

recognized at Lisheen [12,46]. Early framboidal pyrite is only locally observed in Lisheen, sometimes with sphalerite replacement. Pyrite is often noted as being replaced by sphalerite (Figure 6a,e), with fracture infilling by galena (Figure 6g). Minor colloform and dendritic pyrite (Figure 6b) also occur. Texturally and chemically later zoned pyrites are common at Lisheen (Figure 6h)

Sphalerite shows a wide range of textures including colloform, intergrowths with dolomite, replacing pyrite, and as euhedral aggregates. In the Island Pod it displays two main textures; colloform and non-colloform, crystalline sphalerite. Early sphalerite shows colloform texture (Figure 6c) and is often intergrown with ore stage dolomite (Figure 6d). Later sphalerite has been identified as fine-grained euhedral aggregates cementing coarser euhedral pyrite crystals (Figure 6h) and replacing early pyrite (Figure 6a). Several generations have been identified based on color and trace-element chemistry (Figure 6c).

Galena is widely dispersed throughout all the orebodies at Lisheen. Galena can occur as dendritic crystals, filling cavities, by replacement and veining. Galena has been identified from all parts of the mineralization at Lisheen, with early dendritic galena commonly observed in association with colloform sphalerite and/or infilling dolomite (Figure 6f). A later generation occurs as coarser crystals and infillings of open spaces in brecciated late pyrite (Figure 6g). This later galena has been reported associated with Pb sulfosalts [12].

6. Sulfur Isotope Composition

A total of 31 spot analyses of the sulfur isotope composition of pyrite, marcasite, sphalerite, and galena (Figures 7, 8 and Table A1) were carried out on samples from Tara Deep and the TBU, Navan (Figure 7b), and from the Island Pod and Main zone oolite-hosted mineralization, Lisheen (Figure 8b).

6.1. Tara Deep, Navan

A large pre-existing database exists of 390 δ^{34}S values from Navan, covering all styles of mineralization [9,17–19,47]. These analyses reveal three main populations of δ^{34}S in sulfides from –40 to –25‰ (chiefly pyrite, but also sphalerite and galena in the Conglomerate Group Ore); from –25 to –4‰; and from –4 to +17.5‰. Barite values range from +17 to +24‰ (Figure 7a).

Overall, the sulfide δ^{34}S values from the Tara Deep deposit range from –18 to +25‰ (Figure 7b and Table A1) and show a comparable distribution pattern to the Main Navan Orebody (from –40 to +16%; see above). However, S isotope compositions at Tara Deep range to slightly heavier values (up to 25‰) than in the Navan Main Orebody (up to +17.5‰).

δ^{34}S values for sphalerite fall within the range –8.8 to 10.5‰ (mean of +0.6‰; $n = 5$; s.d. = 9.9) (Figure 7b). As noted by Anderson et al. [9] for the Navan deposit, there is a relationship between sphalerite texture, paragenesis, and δ^{34}S value. Paragenetically early sphalerite textures, such as filling interstices in earlier dolomite (Figure 5c), colloforms associated with dolomite (Figure 5d), euhedral aggregates (Figure 5e), and those associated with framboidal or colloform pyrite (Figure 5a,f, and Figure 7b2,b3), generally show negative values (Figure 7b). In contrast, the second generation of sphalerite, including latest infillings (Figure 5h), and those associated with stibnite (Figures 5k and 7b5), shows positive values.

Galena ranges from –9.2 to 9.4‰ (mean of +1‰; $n = 5$; s.d. = 8.6) suggesting also a distribution dependent on texture and paragenesis (Figure 7b). The oldest generation of galena, including skeletal aggregates embedded in colloform pyrite (Figures 5g and 7b2) and galena replacing framboids and colloform pyrite (Figure 5a,g, and Figure 7b3), have negative values. However, the younger generation of galena, such as late infilling in pyrite (Figure 5h) and coarse galena with stibnite and tetrahedrite inclusions (Figures 5i and 7b5), shows positive values.

Tara Deep pyrite δ^{34}S values range from –17.7 to +12.9‰ (mean of +4.2‰; $n = 5$; s.d. = 14.6) and their distribution again correlates with texture and paragenesis (Figure 7b). Primary textures including framboids (Figures 5a and 7b3), colloforms (Figures 5f and 7b2) and pyrite replacing fossils (Figure 5b)

show negative values, whereas later, recrystallized pyrite (Figure 5l) and pyrite replacing marcasite (Figures 5j and 7b4) have positive values.

The δ^{34}S values of marcasite (Figures 5j and 7b4) are generally heavy, ranging from −0.1 to +24.6‰ (mean of +13.5‰; *n* = 5; s.d. = 9), whereas marcasite from Navan Main orebody is more variable, ranging from −37.3 to +17.5‰ (mean of +1.6‰) (Figure 7b).

6.2. TBU, Navan

Framboidal pyrite (Figure 5m,n, and Figure 7b1) within the TBU overlying Tara Deep shows a wide range of negative δ^{34}S values from −37.4 to −8.3‰ (mean of −26.9‰; *n* = 9; s.d. = 11.1) (Figure 7b and Table A1). The δ^{34}S for interstitial sphalerite (Figures 5n and 7b1) is also light with two analyses yielding −32.1 and −32.8‰ (Figure 7b).
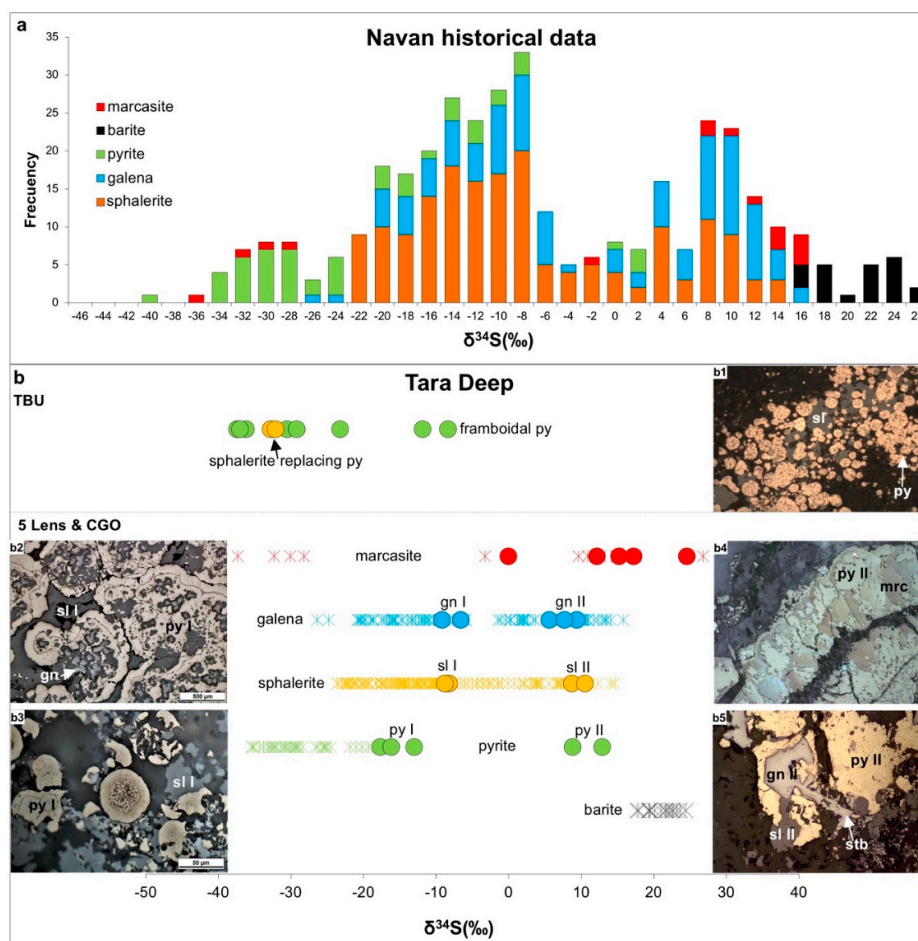
Figure 7. S isotope analyses from the Navan system. (**a**) Histogram showing published S isotope data from the Navan Main Orebody [9,17–19,47]; (**b**) plot distinguishing new S isotope data (Table A1) from the Tara Deep orebody (circles) and published data from the Navan Main Orebody (crosses). New S isotope analyses from Tara Deep including the overlying Thin Bedded Unit (TBU) (**b1**); 5 lens mineralization (**b2–b3**); and Conglomerate Group Ore (CGO) (**b4–b5**). Analyses are compared with mineralogy, textures, and paragenesis. (**b1**) Laminated framboidal pyrite (py) replaced by sphalerite (sl); (**b2**) first generation of sphalerite (sl I) filling open spaces in colloform pyrite (py I); (**b3**) relicts of early framboidal pyrite (py I) partially replaced by colloform pyrite and associated with the oldest sphalerite (sl I) and galena (gn I) generation; (**b4**) marcasite partially corroded and replaced by late pyrite (py II); (**b5**) stibnite (stb) aggregates intergrown with the second generation of sphalerite (sl II) and galena (gn II) and filling open spaces in late pyrite (py II).

6.3. Island Pod and Main Zone, Lisheen

Previous S isotope analysis of samples from Derryville, Main zone, and Bog zone orebodies at Lisheen (n = 119) reveal δ^{34}S values ranging from −44.1 to +11.8‰ (average of −11.6‰). Barite ranges from +14.3 to +18.1 δ^{34}S [12] (Figure 8a). One clear peak in the δ^{34}S distribution pattern is evident (−18 to +6‰). However, the total range for sulfide minerals (−44 to +12‰) is broadly similar to the Navan Main orebody, except that the spectrum appears to be lower by about 5‰, including both the lowest values (pyrite) and the highest values (barite).

δ^{34}S values of pyrite, sphalerite, and galena from the Island Pod and Main zone oolite-hosted mineralization vary from −42.3 to +9‰ (Table A1 and Figure 8b) and fall within the range previously reported for Derryville, Main zone, and Bog zone (Figure 8a,b). In detail, sulfides in the Main zone have δ^{34}S values ranging from −26.3 to +1.5‰ (mean of −9.8‰; *n* = 10; s.d. = 7.4), while the Island Pod shows lighter δ^{34}S values varying from −42.3 to +9‰ (mean of −14.2‰; n = 16; s.d. = 15).

Pyrite shows the widest range, with δ^{34}S values of −42.3 to −7.4‰ (mean of −25.3‰; *n* = 9; s.d. = 11.9). Based on the textures and paragenesis, early pyrite shows a lighter S isotope compositions, while slightly later pyrite, which may be brecciated (Figures 6g and 8b4) and is often seen as euhedral zoned crystals (Figures 6h and 8b3), exhibits relatively high δ^{34}S values.

Sphalerite δ^{34}S values range from −14.4 to +1.5‰ (mean of −6.8‰; *n* = 10; s.d. = 4.5). Early colloform sphalerite and later crystalline varieties from the Island Pod have indistinguishable δ^{34}S values. However, for other Lisheen orebodies, previous researchers [12] reported δ^{34}S variation based on texture, with non-colloform varieties typically showing a larger spread in δ^{34}S value, while colloform sphalerite was typically focused around −11 ‰.

The δ^{34}S of galena varies from −13.9 to +9‰ (mean of −2.9‰; *n* = 5; s.d. = 9).
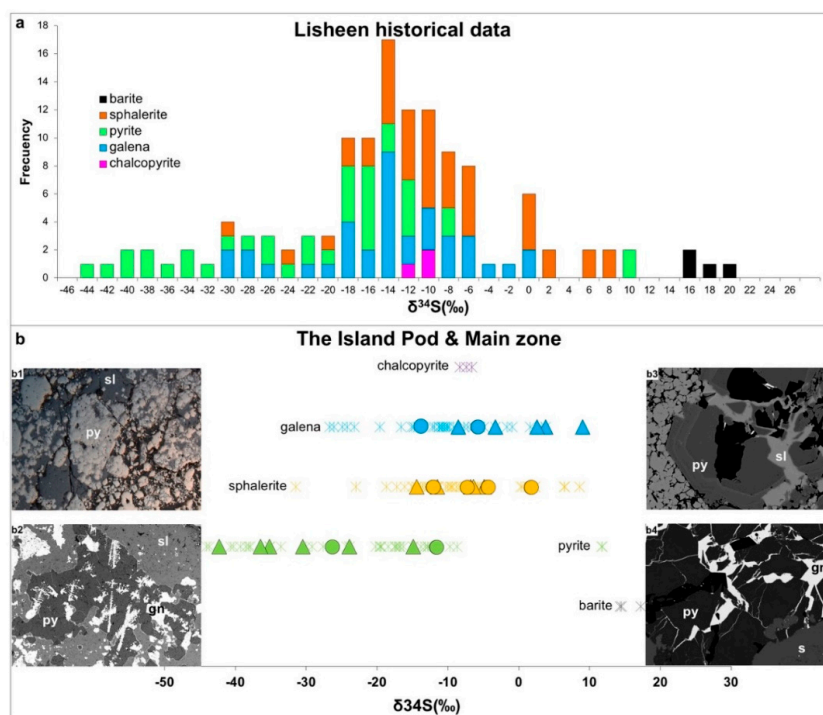
Figure 8. S isotope analyses from the Lisheen system. (**a**) Histogram showing published S isotope data [12]; (**b**) plot distinguishing new S isotope data (Table A1) from the Island Pod (IP) (triangles) (**b1,b3,b4**); Main zone oolite-hosted (MZ) (circles) (**b2**) and published data from Main zone (crosses). New S isotope analyses are also compared with mineralogy, textures, and paragenesis. (**b1**) Early pyrite (py) partially replaced by the later sphalerite (sl); (**b2**) early dendritic galena (gn) associated with pyrite; (**b3**) early zoned, euhedral pyrite, with fracture infilling by the later sphalerite; and (**b4**) late fracture-filling galena in massive pyrite.

7. C–O Isotope Composition

Carbon and oxygen isotope data from carbonate phases in Irish-type deposits have been used to constrain fluid processes associated with ore formation [43,48,49].

7.1. Navan

At Navan, C and O isotope data have been reported by Braithwaite [48], Pearce [49] and Ashton et al. [11]. In addition, 14 new analyses are presented from late carbonate veins (Figure 9a and Table A2) from NW of the Randalstown Fault, which contain coarse honeyblende sphalerite, most likely remobilized from the SWEX orebody. Ashton et al. [11] provide a review of the carbonate paragenesis and C–O isotope data of the whole Navan deposit, summarized briefly here.

Dolomitization at Navan was not as extensive as at Lisheen, with much of the host stratigraphy remaining un-dolomitized. A plume-shaped body of dolomitization in the NW portion of the Main Orebody [48] extends in an ENE direction with stratal fingers along sandy and silty grainstone lithologies [11]. Based on fluid inclusion and C–O isotopic data it was interpreted as hydrothermal in origin, most likely reflecting upwelling basinal brines that became hotter (~60 to 160 °C) with time [48]. The plume also connects with stratiform dolomite layers which locally form the hanging wall to some ore lenses and thus predate mineralization [11]. Following early dolomitization, sulfide deposition occurred synchronously with further calcite and dolomite precipitation [49].

The ranges of C and O isotope ratios for Navan carbonates (Figure 9a) are in most respects similar to those for Lisheen. Most analyses of early dolomite phases at Navan (e.g., 5 lens dolomite, massive dolomite) lie close to the host stratigraphy $\delta^{13}C$ and $\delta^{18}O$ values (i.e., Pale Beds Group), except that they extend to lower $\delta^{18}O$. Early dolomitization at Navan is marked by slightly lower $\delta^{13}C$ (−1 to 3‰) than at Lisheen (2–3‰). This is particularly true for samples of "massive dolomite" from the core of the plume. Syn-mineralization carbonate phases at Navan show considerable scatter across the several stages identified (Figure 9a) with comparable $\delta^{18}O$ values to early dolomites, but extending to negative $\delta^{13}C$ values. Post-ore late calcite veins from Navan show the largest range of $\delta^{18}O$ (from 15 to 26‰) with restricted $\delta^{13}C$ (−2.6 to 1.8‰).

7.2. Lisheen

Published C and O isotope data from the Lisheen deposit [43,50] and 20 new analyses are presented (Table A2, Figure 9b). The following broad carbonate sequence is well established [45,50]. As already mentioned, early "regional dolomitization" of the host stratigraphy comprises two phases, D_{1a} and D_{1b}, that replace micritic components of the host Waulsortian Limestone (Figure 6j). Mineralization at Lisheen is related to a later hydrothermal dolomitization resulting in two main ore-related dolomites: D_2-BMB, which hosts most of the economic mineralization (Figure 4h), and D_3-WMB (Figure 4i). A number of ore-stage carbonate phases are commonly intergrown with sulfides [24,45]. Following the main period of mineralization, the following carbonate generations have been recognized (in order): White ferroan dolomite (D_4), pink saddle dolomite (D_5), and late calcite (C_6).

Available C and O isotope data for the Lisheen carbonate phases are shown in Figure 9b. The undolomitized Waulsortian Limestone Formation across Ireland (e.g., Tynagh, Togher, Ballycudduhy) is characterized by $\delta^{18}O$ values of 22.2 to 28.4‰ and $\delta^{13}C$ values of 2.9 to 4.1‰, typical of Carboniferous marine carbonates. Samples of early pale grey replacive regional dolomite (D_{1a}) at Lisheen yield slightly lower $\delta^{18}O$ values (mean 23.9‰; range 22.2–26.0‰). Subsequent coarser white regional dolomite (D_{1b}) yields still lower values (mean 22.3‰; range 19.5–25.1‰). However, the appearance of BMB (D_2) is marked by a return to high $\delta^{18}O$ values (similar to D_{1a}), whereas white dolomite of the WMBs (D_3) is more similar to D_{1b}. Post-ore carbonates are marked by a range of $\delta^{18}O$ values, which are predominantly low and comparable to WMBs. Significant variation in $\delta^{13}C$ at Lisheen only occurs in post-ore phases, which are marked by negative values (to −6.5‰).
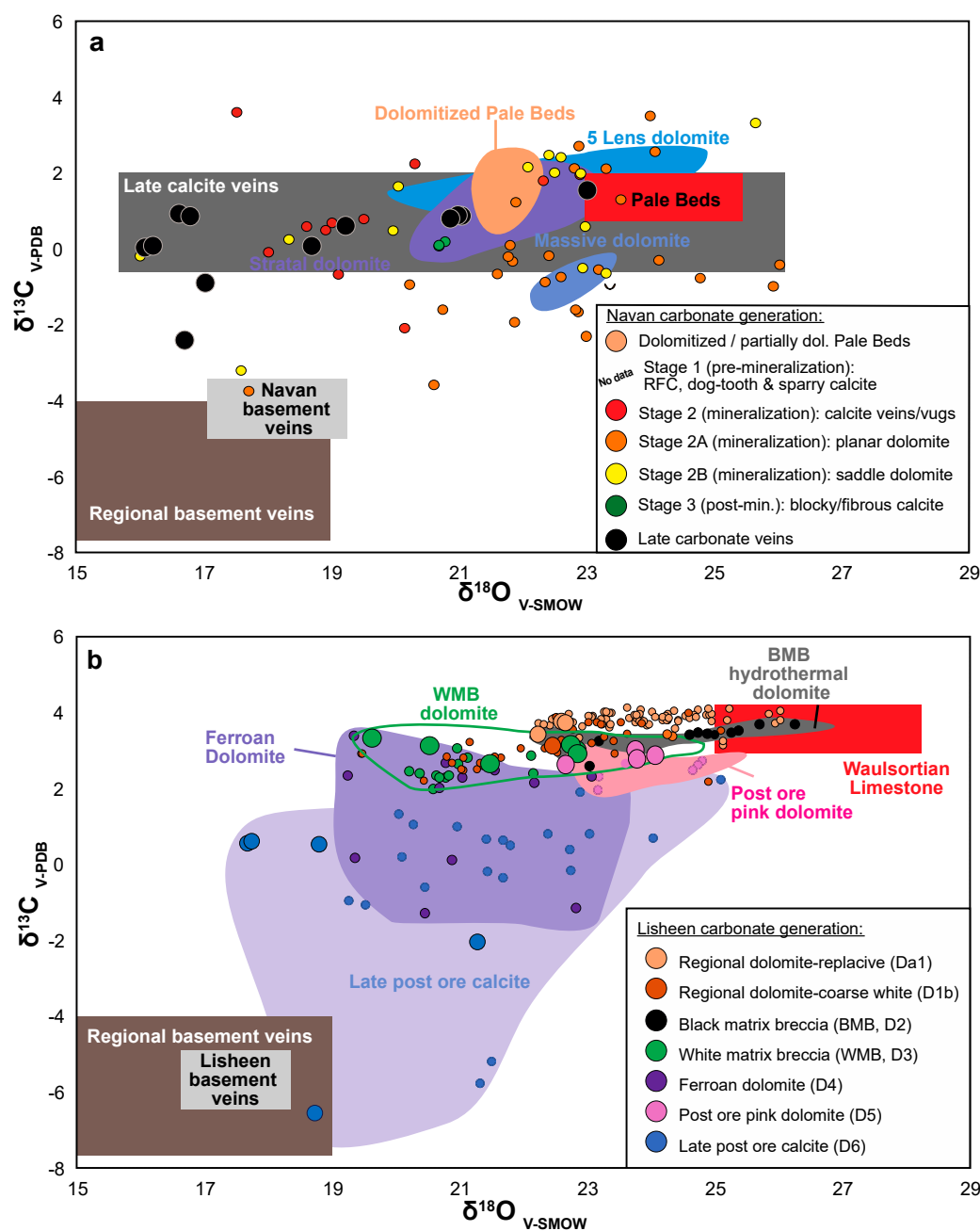
Figure 9. C and O isotope compositions of carbonates from the Navan (**a**) and Lisheen (**b**) deposits, expressed conventionally as $\delta^{13}C$ and $\delta^{18}O$ values. New data (Table A2) are shown as larger symbols; small symbols include historical data associated with mineralization; and shaded fields represent historical data associated with both dolomitized and un-dolomitized Pale Beds to improve the clarity of the figure [11,43,48–50].

8. Pb Isotopes

8.1. Navan

Twelve high-precision additional analyses from Tara Deep Pale Beds and Conglomerate-hosted mineralization, Tatestown, and the Navan Main Orebody have been obtained for comparison with existing data from the Navan system (Figure 10, Table A3). Overall, high-precision galena Pb isotope analyses show a homogenous composition with mean $^{206}Pb/^{204}Pb$, $^{207}Pb/^{204}Pb$, and $^{208}Pb/^{204}Pb$ ratios of 18.2197, 15.5802, and 38.0811, respectively.

8.2. Lisheen

Although values are broadly similar to those obtained from Navan, $^{207}Pb/^{204}Pb$ and $^{206}Pb/^{204}Pb$ ratios are slightly higher, and the degree of homogeneity is striking. However, with the improved precision of 37 new analyses (Table A3, Figure 10), subtle isotopic differences have now been noted between the various ore lenses (i.e., Main zone, Derryville, Bog zone, Island Pod). This variation is within error of previously published analyses [20,24], with the most variation and lowest average Pb isotope ratios in the largest lenses [38]. In general terms, galena Pb isotope analyses exhibit consistent composition and mean $^{206}Pb/^{204}Pb$, $^{207}Pb/^{204}Pb$, and $^{208}Pb/^{204}Pb$ ratios of 18.1938, 15.5941, and 38.0630, respectively.
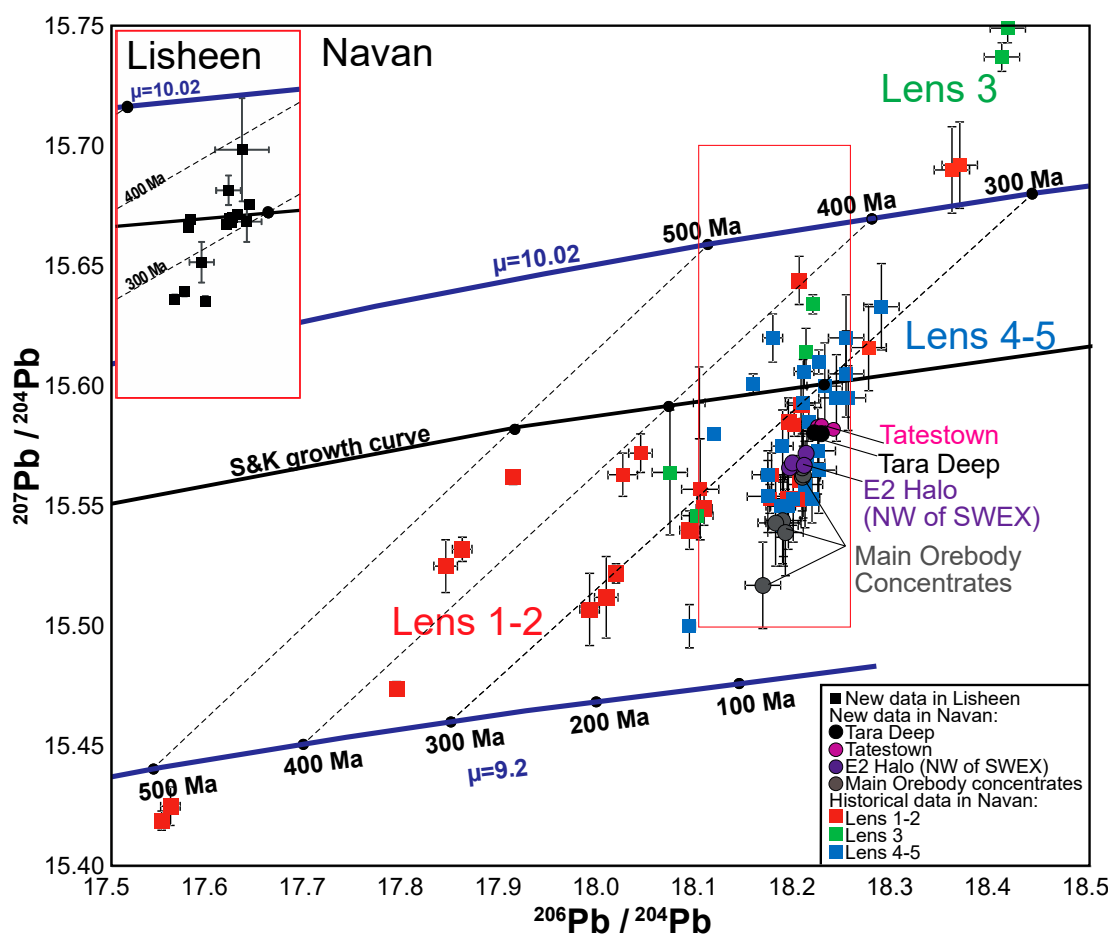
Figure 10. $^{206}Pb/^{204}Pb$ and $^{207}Pb/^{204}Pb$ isotope constraints from the Navan and Lisheen deposits. New Lisheen data (black squares) are shown inset for clarity, new Navan data as colored circles (range shown by the right-hand red box) and published Navan data as colored squares [17,21,24,51–53].

9. Discussion

9.1. Metal sources

In the past three decades it has become increasingly apparent that individual Irish-type deposits display remarkably homogeneous Pb isotope compositions, which vary systematically across Ireland. Ratios of $^{206}Pb/^{204}Pb$, $^{207}Pb/^{204}Pb$ and $^{208}Pb/^{204}Pb$, calculated $\mu(^{238}U/^{204}Pb)$ and model ages can be contoured to reflect variations in basement sources from which metals were derived [54,55]. Galena from Precambrian and Lower Palaeozoic mesothermal gold, volcanogenic massive sulfide and SEDEX occurrences in NW Ireland are characterized by a μ value of 9.2 (reflecting Laurentian-affinity crust). Similar Lower Palaeozoic-hosted galena occurrences in SE Ireland plot along a trend with a μ value

of ~10, typical of Ganderian-Avalonian basement. A source of Pb from the Old Red Sandstone has been ruled out by Everett et al. [54] on isotopic grounds. Within the Longford–Down Terrane that runs across the centre of Ireland, data from both Carboniferous-hosted Zn–Pb deposits and Lower Palaeozoic basement veins (their purported feeders) form linear arrays between these end-member curves [55], suggesting mixed Pb sources. The majority of Pb for Irish base metal deposits was most likely derived from lower Palaeozoic Ganderian-Avalonian basement with probably a minor Laurentian component [54–56]. The lack of Pb isotope variation in new data for Lisheen (Table A3, Figure 10) is consistent with existing published results [21,24] and with the regional variation exhibited by the other Irish deposits [55]. This suggests a relatively well-homogenized crustal reservoir and a common Pb source at Lisheen (Figure 10). Subtle Pb isotope variations between ore lenses may reflect contamination upon ascent, and is the focus of ongoing research.

Navan is unusual in the Irish Midlands as large isotopic differences have been noted between the different ore lenses (Figure 10). Mills et al. [52] proposed in their study of the Main Orebody, that while the Pb isotope composition was relatively homogeneous in the lower ore lenses (3 to 5), increasingly unradiogenic signatures occur in the upper lenses (1 and 2) (Figure 10). This was suggested to represent a tapping of progressively deeper sections of the underlying crust [52]. New analyses of samples from the Main Orebody (Table A3) have not confirmed any such variation between the ore lenses, with all values clustered near those from the SWEX epigenetic halo [53], Tara Deep Pale Beds and Conglomerate-hosted mineralization, Tatestown occurrence, and the Navan Main Orebody concentrates (Table A3 and Figure 10). The significant scatter of ratios in the [52] dataset may be a consequence of instrument mass fractionation during TIMS analysis. We propose that Pb isotope variations at Navan are likely to be subtle as at Lisheen, though this has yet to be tested by detailed analyses.

Regarding the transport mechanism for metals in Navan and Lisheen, this process may be comparable with those reported by Bischoff et al. [57], who demonstrated by laboratory tests that heated brines can leach considerable amount of metals from Lower Palaeozoic greywackes to form Irish-type orebodies. This is consistent with fluid inclusion data reviewed by Wilkinson et al. [58], indicating that metal-bearing fluids could be derived from partially evaporated seawater. Following the convection cell model of Russell [59], Irish-type deposits have been proposed to be the result of brines that descended into the Lower Palaeozoic basement, where they leached metals and were heated, subsequently rising along normal faults below the developing deposits [13]. In addition, reactivation of normal faults, related to on-going extensional activity, together with cyclicity in sulfide deposition, indicate a superposition of mineralizing fluid pulses at both Navan and Lisheen [11,25].

By analogy with other SEDEX ore deposits, elevated concentrations of some metals and metalloids (Cu, Co, Ni, As, and Sb) within the deposits can be associated spatially with feeder zones; these elements are typically more abundant close to vent systems [60]. At Lisheen (Figure 4a), Cu, Co, Ni, and As are more abundant within the oolite-hosted mineralization closer to the major structures [20,24,25]. The association of these elements with these major EW faults supports the hypothesis that they were the pathways for hydrothermal metal transport during ore formation. This is consistent with strong leaching of the basement rocks observed close to the main fault zones at Lisheen [10]. The regional metal distribution across the different orebodies at Lisheen suggests that the Island Pod, which has especially low Cu, Co, Ni, and As, is a distal orebody to the main feeder(s). This is also consistent with low trace metal signatures (e.g., Cd, Co) in Island Pod sphalerite [46].

The Tara Deep deposit shows higher Cu and Sb concentrations as stibnite, tetrahedrite, and chalcopyrite (Figure 5i,k,l) than the Navan Main Orebody and SWEX. This metal distribution pattern suggests that Tara Deep is situated proximal to a significant feeder region within the Navan system, likely the S fault (Figure 2a). In Tara Deep, the circulation of metal-bearing fluids continued during the deposition of the Lower Visean sedimentary breccias (Figures 2b and 4e) and the immediately overlying TBU (Figures 2b and 4f). Significant amounts of marcasite in the mineralized conglomerate

(Figure 4e) and the large amount of laminated pyrite, with low Zn and Pb concentrations, within the TBU (Figure 4f) suggest that TBU mineralizing fluids were progressively exhausted in Zn and Pb.

9.2. Sulfur Sources

Barite δ^{34}S values reported for both Lisheen (mean of 16‰) and Navan (mean of 21‰) [6,24] are comparable to Lower Carboniferous seawater sulfate. This suggests that contemporaneous seawater was the source of sulfate for barite at Navan and Lisheen.

In Irish-type deposits, the distribution of S isotope compositions in sulfides is interpreted as the mixing of two different sulfur sources. Negative δ^{34}S values in sulfides have been classically interpreted as the result of bacteriogenic reduction of Lower Carboniferous seawater sulfate in an open system [3,9,17,18,47,61]. For example, early framboidal and colloform pyrite in both Navan (Figure 5l,f) and Lisheen (Figure 6a) have δ^{34}S values as light as −40 and −44.1‰, respectively, representing a fractionation of ~60‰ from seawater sulfate. This extreme fractionation can only be explained by bacterial sulfate reduction (BSR) [61,62].

Available sphalerite and galena δ^{34}S data from Tara Deep suggest a comparable bimodal distribution pattern to the Navan Main Orebody (Figure 7a,b). The two main peaks at −10 and 10‰ suggest two separate sources of sulfur. Early colloform and euhedral aggregates of sphalerite (Figure 5d–f), alongside early skeletal galena, and galena replacing pyrite (Figures 5a,g, and 7b2), display negative δ^{34}S values. The correlation of these negative δ^{34}S values with rapid crystallization textures (Figure 7b) suggests that mixing of two fluids, one bearing metals and the other carrying bacteriogenic sulfide, was the local trigger for sulfide deposition [3]. The group with positive δ^{34}S values (10‰) is associated with late interstitial sphalerite and galena with stibnite exsolutions (Figures 5h,i,k, and 7b5). These textures and associated S isotope results have been related to periods of intense hydrothermal activity, where sulfide precipitation occurs through changing P-T conditions, creating supersaturated conditions and reducing the buoyancy of the metal-bearing, hydrothermal fluid [11,18]. In contrast to the Navan Main Orebody, pyrite in Tara Deep displays a bimodal δ^{34}S distribution (Figure 7b), similar to sphalerite and galena. This pattern suggests again two different sulfur sources, BSR associated with framboidal and colloform pyrite (Figure 5a,f) and thermal reduction related to recrystallized pyrite (Figure 5j). However, marcasite in Tara Deep displays an exclusively positive range of δ^{34}S values, suggesting that marcasite precipitation occurs only in periods of intense hydrothermal activity. It is also worth noting the trend toward higher δ^{34}S values in Tara Deep (up to 25‰) compared to the Main Navan Orebody (up to 17.5‰) (Figure 7a,b). This, in conjunction with the higher abundance of Cu and Sb minerals at Tara Deep (Figure 5i,l), suggests that there were more intense pulses of hydrothermal fluid at Tara Deep.

The uneconomic TBU mineralization, that overlies the main Tara Deep deposit, hosts both laminated framboidal pyrite and associated sphalerite (Figure 5m,n). These textures reveal negative δ^{34}S values, suggesting a BSR origin for sulfide, possibly during early diagenesis.

At Lisheen, the predominance of negative δ^{34}S values in all the generations of sphalerite and galena (main peak at −14‰) supports a BSR sulfur source for the main mineralization stages (Figure 8a,b), as previously proposed [24]. However, some higher δ^{34}S values (up to 12‰), relating to paragenetically late textures, such as replacive galena (Figure 6g,h), suggest a minor hydrothermal source for sulfur. In addition, spatial variations in S isotope compositions throughout the Lisheen orebodies can also be associated with feeder zones. In that sense, the lower δ^{34}S values from the Island Pod compared to the Main zone support the notion that the Island Pod is a distal orebody to the main Lisheen feeder.

9.3. C–O Isotopes

The C–O isotope variations at Lisheen can be explained primarily through processes of fluid-rock buffering [50]. Although the exact cause for early regional dolomitization is not known, measured δ^{18}O values are consistent with fluid of high δ^{18}O and temperatures of formation (~150–200 °C), confirmed by clumped C–O isotope analyses [37,38]. It is perhaps no surprise that δ^{18}O values for

subsequent black hydrothermal dolomite from BMBs are similar to that recorded by corroded clasts of the fine-grained regional dolomite that it contains (Figure 9a). Dolomite in WMBs most likely formed as hydrothermal infills to collapse breccia associated with significant dissolution of the underlying Waulsortian limestones [45]. Measured carbonate mineral $\delta^{18}O$ values are a function of high but varying temperatures and fluid $\delta^{18}O$ values buffered by surrounding carbonate rocks [50]. Post-ore carbonate phases formed at low temperatures, typically < 40–125 °C [28,41]. Basement veins at Lisheen have yielded low $\delta^{18}O$ values (16.7–18.4‰) and strongly negative $\delta^{13}C$ values (−5.1 to −5.7) ‰) [50]. These results are consistent with fluids that have not been buffered by Carboniferous limestones.

At Navan, as at Lisheen, dolomitization of the host stratigraphy is marked by a reduction in $\delta^{18}O$ (Figure 9b). Published $\delta^{18}O$ values for different dolomite lenses are similar with the notable exception of parts of the 5-lens dolomite. Ore stage carbonates from across the deposit show considerable scatter in $\delta^{18}O$ reflecting a combination of variations in temperature, local rock buffering (by carbonates with different $\delta^{18}O$ values), the presence of in situ pore waters, and/or varying fluid/rock ratios [11]. Late calcite veins (~80–110 °C) that contain remobilized sulfides are marked by extremely variable $\delta^{18}O$ (16–26‰), suggesting local rock buffering.

9.4. Controls on Metal Deposition

Similar to the Navan Main Orebody, the permeability of the host rock at Tara Deep exerted an important control on the mineralizing processes. In that sense, owing to its low compressive strength and high calcite content, the micrite was susceptible to fracturing and replacement. The high density of mineralized minor fractures in the Micrite Unit (Figures 2b and 3a–c) suggests that secondary permeability was developed during extension and hydraulic fracturing by pressurized hydrothermal fluids [11]. The circulation of acidic mineralizing fluids through these hydraulic fractures resulted in dissolution of carbonates leading to enhanced porosity/permeability and the buffering of the mineralizing fluids [9]. In addition, the presence of detrital sulfide clasts in debris flows above the Lower Visean erosional surface, that are later encased by mineralization, suggests that metalliferous fluids entered the system prior to the formation of those sedimentary breccias.

Uneconomic mineralization within the overlaying TBU is hosted by dark mudstone layers (Figures 2b and 3f). Here, the close relationship between organic matter and laminated framboidal pyrite suggests that this style of mineralization was generated by the replacement of soft sediments during early diagenesis and close to the seawater-sediment interface. The presence of laminated pyrite at these higher stratigraphic levels suggests that the mineralization process continued over a longer period at Tara Deep.

Compared to Navan, the Lisheen deposit is hosted at higher stratigraphic levels within the Tournasian sequence (Figure 4b). Mineralization mainly replaces hydrothermal dolomite breccias developed in the Waulsortian mud banks (Figure 3h,i) and to a lesser extent, the Lisduff Oolite Unit of the Ballysteen Limestone Fomation (Figure 4b). At Lisheen, regional dolomitization of the Waulsortian prior to the sulfide mineralization event resulted in a significant increase in porosity and permeability. According to Hitzman et al. [10] the development of this secondary permeability exerted an important control on the mineralizing processes. In that sense, hydrothermal mineralizing fluids circulated throughout the dolomitized Waulsortian rocks, resulting in the brecciation and sulfide deposition (Figure 3h,i). Textures suggest that in the first stages, sulfides replaced the BMB, followed by the replacement of the regional dolomite clasts in later mineralization stages. As proposed for Navan, the circulation of acidic mineralizing fluids resulted in the dissolution of carbonates and precipitation of sulfides, primarily by reaction of bacteriogenic sulfide with metal-bearing fluids.

At both Navan and Lisheen, the clear association between major normal faults and metal distribution indicates strong structural control [10,11,18,25]. For example, Tara Deep is situated in the hanging wall of the ENE-trending G fault and the footwall of the Navan fault (Figure 2a). The structural terrace formed by the G and Navan faults is cut by the NNW-striking S fault (Figure 2a) and mineralization in the NW zone of Tara Deep seems to be focused in the area where the S Fault

encroaches on the G Fault to the north, and the Navan Fault to the south [13]. Likewise, Lisheen is associated with relay-ramp zones along a complex fault system (Figure 3a). The location of the orebodies, metal distribution, and the related hydrothermal alteration with proximity to likely feeder zones is evidence that hydrothermal fluids were able to circulate along EW faults and minor faulting in the relay zones [10].

9.5. Implications for Exploration

The economic regions of Irish-type Zn–Pb deposits are becoming increasingly well understood. However, much less attention has so far been paid to the exploration value, for vectoring purposes, of sub-economic sulfide halos surrounding the deposits. Laminated pyrite hosted in the TBU overlying the Tara Deep deposit suggests that hydrothermal fluids that formed Tara Deep were able to reach the seafloor, with the potential for forming sedimentary-exhalative (SEDEX) mineralization [63]. Nevertheless, linkages between these halos and the Navan mineralization remain poorly understood. Understanding these links has the potential to dramatically enhance mineral exploration strategies for deeply buried deposits, as well as to strengthen genetic models of both epigenetic and SEDEX mineralization.

Ongoing research into exploration methods for vectoring towards Irish-type and related SEDEX deposits include the study of mineralogical and textural patterns and associated chemical and isotopic zonation, where possible, by means of micro-analytical methodologies. Laser ablation inductively coupled plasma-mass spectrometry (LA-ICP-MS) has been extensively applied in the evaluation of trace elements in sulfides, mainly in pyrite, and applied to exploration [64]. Sulfide trace element compositions, especially of pyrite, can be used to constrain sources of metals, fluid pathways and mixing sites as well as acting as a vectoring tool [64].

10. Conclusions

The data presented in this study suggests that the Tara Deep and Island Pod deposits closely resemble the Navan and Lisheen deposits, respectively. Common features include: Tectonic setting, main mineralogy, nature of host rock, and mineralization affinity. The main differences are centered on the geochemistry, dealing essentially with metal distributions, such as enrichment in Sb and Cu. At Tara Deep, elevated Sb and Cu suggest proximity to a major feeder system; while depletion in Cu, Co, and Ni in the Island Pod, in comparison to Lisheen, suggest a distal relationship to the feeder system.

Although the major mineralogy of Tara Deep and Island Pod deposits are similar to those of the Navan and Lisheen orebodies, respectively, there are differences regarding minor mineralogy. In Tara Deep, stibnite, tetrahedrite, and chalcopyrite host Sb and Cu enrichments and are interpreted as resulting from proximity to a feeder zone. In contrast, the lack of chalcopyrite and Ni-sulfosalts in the Island Pod, in comparison to Lisheen, suggest a position distal to major hydrothermal feeders.

Regarding S isotope compositions, both Tara Deep and the Island Pod show similar patterns to Navan and Lisheen, respectively. However, in detail, Tara Deep has slightly heavier δ^{34}S values relative to Navan, suggesting either a larger input of hydrothermal H_2S, or a reduced level of BSR. In contrast, the Island Pod shows lighter δ^{34}S values than Lisheen, implying an increased BSR S source, or decreased hydrothermal fluid circulation.

C and O isotope data at Lisheen reveal a relatively simple fluid evolution, whereas the situation at Navan is far more complex. At Lisheen, carbonate δ^{18}O is dominated by fluid-rock buffering by early regional dolomite at a range of temperatures. More negative δ^{13}C values for post-ore phases are due to interaction with inorganic matter. Basement veins at Lisheen have yielded low δ^{18}O values and strongly negative δ^{13}C values consistent with fluids that have not been buffered by Carboniferous limestones. At Navan, carbonate phases across the system show extremely variable δ^{18}O and δ^{13}C values, reflecting a combination of variable temperature of carbonate formation, local host rock buffering, the presence of in situ pore waters, and/or varying fluid/rock ratios.

The homogeneity of the new Pb isotope analyses for Navan and Lisheen is consistent with published data for other Irish deposits, suggesting a local crustal reservoir dominated by Lower Palaeozoic rocks. The new high-precision analyses from several Navan orebodies do not confirm the large variations in previously published data, suggesting that the Pb isotope ratios of the metal-bearing fluid is much more homogeneous than previously considered.

The identification of geochemical halos surrounding the Tara Deep deposit confirms the potential to develop vectors towards undiscovered mineralization.

Appendix A

Table A1. S isotope data from Tara Deep, TBU (Navan) and Main zone and Island Pod (Lisheen).

Sample ID	Mineralization	Mineral	Texture	δ^{34}S (‰)
			Navan Deposit	
			Tara Deep orebody	
N02437/08	Micrite hosted	Sphalerite	Massive	−8.3
N02427/04	Micrite hosted	Sphalerite	Massive	−8.2
N02437/01	Micrite hosted	Sphalerite	Massive	−8.8
N02334/07	Micrite hosted	Sphalerite	Massive	+8.7
N02370/05	Micrite hosted	Sphalerite	Laminated	+10.5
N02427/04	Micrite hosted	Galena	Coarse	−9.2
N02437/03	Micrite hosted	Galena	Coarse	−6.6
N02334/07	Micrite hosted	Galena	Coarse	+5.6
N02370/05	Micrite hosted	Galena	Disrupted coarse	+9.4
N02445/05	Micrite hosted	Galena	Disrupted interstitial	+7.7
N02428/06	Micrite hosted	Pyrite	Euhedral	−17.7
N02428/04	Micrite hosted	Pyrite	Colloform	−16.2
N02428/04	Micrite hosted	Pyrite	Colloform	−13
N02437/02	Micrite hosted	Pyrite	Veinlet	+8.8
N02437/03	Micrite hosted	Pyrite	Euhedral recrystallized	+12.9
N02409-17a	Mineralized conglomerated	Marcasite	Colloform	−0.1
N02409-17b	Mineralized conglomerated	Marcasite	Radial	+15.2
N02409-17c	Mineralized conglomerated	Marcasite	Replacing pyrite	+24.6
N02439-5a	Mineralized conglomerated	Marcasite	Radial	+12.1
N02439-5b	Mineralized conglomerated	Marcasite	Radial	+17.2
			TBU	
N02409-1a	Laminated pyrite	Pyrite	Framboidal pyrite	−36.2
N02409-1b	Laminated pyrite	Pyrite	Framboidal pyrite	−37.3
N02409-1c	Laminated pyrite	Pyrite	Framboidal pyrite	−37.4
N02409-8a	Laminated pyrite	Pyrite	Framboidal pyrite	−11.9
N02409-8b	Laminated pyrite	Pyrite	Framboidal pyrite	−8.3
N02439-4a	Laminated pyrite	Pyrite	Framboidal pyrite	−30.5
N02439-4b	Laminated pyrite	Pyrite	Framboidal pyrite	−37.0
N02439-4c	Laminated pyrite	Pyrite	Framboidal pyrite partially recrystallized	−29.2

Table A1. *Cont.*

Sample ID	Mineralization	Mineral	Texture	δ^{34}S (‰)
N02439-4d	Laminated pyrite	Pyrite	Framboidal pyrite partially recrystallized	−23.2
N02409-1d	Laminated pyrite	Sphalerite	Sphalerite replacing framboidal pyrite	−32.8
N02409-1e	Laminated pyrite	Sphalerite	Sphalerite replacing framboidal pyrite	−32.1
Lisheen deposit				
Island Pod orebody				
ALD025	BMB	Pyrite	Coarse	−35.2
ALD013	BMB	Pyrite	Recrystallized	−23.9
ALD002A	BMB	Pyrite	Dendritic	−14.9
ALD103	BMB	Pyrite	Coarse	−30.4
ALD038	BMB	Pyrite	Dendritic	−42.3
ALD051	BMB	Pyrite	Colloform	−36.4
ALD052A	BMB	Sphalerite	Interstitial in pyrite	−11.5
ALD107	BMB	Sphalerite	Interstitial in pyrite	−14.4
ALD002A	BMB	Sphalerite	Interstitial in pyrite	−6.8
ALD075	BMB	Sphalerite	Euhedral	−4.8
ALD103	BMB	Sphalerite	Interstitial in pyrite	−6.3
ALD013	BMB	Galena	Interstitial in pyrite	−3.3
ALD106	BMB	Galena	Interstitial in pyrite	−3.3
ALD015	BMB	Galena	Interstitial in pyrite	+2.6
ALD016	BMB	Galena	Interstitial in pyrite	+9.0
ALD051	BMB	Galena	Interstitial in pyrite	−8.5
Main zone orebody				
SPL086	Oolite (Ramp zone)	Pyrite	Dendritic	−12.2
SPL088	Oolite (Ramp zone)	Pyrite	Coarse	−7.4
SPL037	Oolite (Ramp zone)	Pyrite	Colloform	−26.3
SPL040	Oolite (Ramp zone)	Sphalerite	Colloform	−12.0
SPL040	Oolite (Ramp zone)	Sphalerite	Colloform	−6.9
SPL040	Oolite (Ramp zone)	Sphalerite	Interstitial in dolomite	−7.3
SPL025	Oolite (Ramp zone)	Sphalerite	Interstitial in pyrite	+1.5
SPL086	Oolite (Ramp zone)	Sphalerite	Replacive	−4.5
SPL088	Oolite (Ramp zone)	Galena	Replacive	−4.7
SPL092	Oolite (Ramp zone)	Galena	Dendritic	−13.9

Table A2. C–O isotope data from Navan and Lisheen deposits.

Sample ID	Location	Carbonate Phase	Mineral	δ^{13}C (VPDB)	δ^{18}O (VSMOW)
Navan Deposit					
A1	NW of Randalstown Fault	Remobilised sphalerite vein	Calcite	0.1	16.9
A2a	NW of Randalstown Fault	Remobilised sphalerite vein	Calcite	0.7	15.9
A2b	NW of Randalstown Fault	Remobilised sphalerite vein	Calcite	0.7	15.9
A2c	NW of Randalstown Fault	Remobilised sphalerite vein	Calcite	0.7	16.0
15a	NW of Randalstown Fault	Remobilised sphalerite vein	Calcite	1.3	16.6
15b	NW of Randalstown Fault	Remobilised sphalerite vein	Calcite	1.3	16.4
16a	NW of Randalstown Fault	Remobilised sphalerite vein	Calcite	1.4	20.6
16b	NW of Randalstown Fault	Remobilised sphalerite vein	Calcite	1.4	20.8
16c	NW of Randalstown Fault	Remobilised sphalerite vein	Calcite	1.4	20.8
25	SWEX	E2 epigenetic halo	Calcite	1.8	22.8
Beaupark	Beaupark	Late carbonate fill to chalcopyrite bearing quartz vein	Calcite	1.2	19.1
2378-1540	Basement vein	Late carbonate fill to chalcopyrite bearing quartz vein	Calcite	−2.6	14.7
2378-1520A	Basement vein	Late carbonate fill to chalcopyrite bearing quartz vein	Calcite	−0.7	16.6
2378-1520B	Basement vein	Late carbonate fill to chalcopyrite bearing quartz vein	Calcite	0.8	18.5

Table A2. *Cont.*

Sample ID	Location	Carbonate Phase	Mineral	δ^{13}C (VPDB)	δ^{18}O (VSMOW)
		Lisheen deposit			
SPL053D	Main zone	White matrix breccia	Dolomite	3.1	20.5
SPL056A	Main zone	White matrix breccia	Dolomite	2.6	21.4
SPL056B	Main zone	White matrix breccia	Dolomite	3.1	22.7
SPL058	Main zone	White matrix breccia	Dolomite	3.0	22.8
SPL060	Main zone	White matrix breccia	Dolomite	3.3	19.6
SPL070	Main zone	Early calcite overprinted by massive pyrite	Calcite	−1.9	22.1
SPL053A	Main zone	Late yellow calcite	Calcite	−6.5	18.7
SPL073	Main zone	Late yellow calcite	Calcite	−2.0	21.2
SPL053Ca	Main zone	Post ore pink dolomite	Dolomite	2.6	23.6
SPL053Cb	Main zone	Post ore pink dolomite	Dolomite	2.8	23.9
AFI032a	Main zone	Post ore pink dolomite	Dolomite	2.9	23.5
AFI032b	Main zone	Post ore pink dolomite	Dolomite	2.9	23.6
SPL049	Main zone	Post ore pink dolomite	Dolomite	2.7	22.6
SPL053Ba	Main zone	Late white calcite vein	Calcite	0.5	17.2
SPL053Bb	Main zone	Late white calcite vein	Calcite	0.5	17.1
D1A1a	7km SE Main zone	Regional dolomite—fine replacive grey	Dolomite	3.7	22.7
D1A1b	7km SE Main zone	Regional dolomite—fine replacive grey	Dolomite	3.7	22.6
D1B1	7km SE Main zone	Regional dolomite—coarse white	Dolomite	3.2	22.4
SPL053Ea	Main zone	Regional dolomite—fine replacive grey	Dolomite	3.4	22.1
SPL053Eb	Main zone	Regional dolomite—fine replacive grey	Dolomite	3.4	22.1

Table A3. Pb isotope composition from Navan and Lisheen deposits.

Sample ID	Orebody	Unit	^{206}Pb/^{204}Pb	^{207}Pb/^{204}Pb	^{208}Pb/^{204}Pb
		Navan			
Pb37	Tatestown	Pale Beds	18.2211	15.5830	38.0863
Pb38	Tatestown	Pale Beds	18.2206	15.5831	38.0847
Pb39	Tatestown	Pale Beds	18.2250	15.5836	38.0896
Pb40	Tatestown	Pale Beds	18.2370	15.5820	38.0934
Pb71	SWEX	Epigenetic halo	18.2030	15.5737	38.0600
Pb44	Tara Deep	Pale Beds	18.2199	15.5792	38.0819
Pb29	Tara Deep	Pale Beds	18.2249	15.5797	38.0885
Pb56	Tara Deep	Pale Beds	18.2047	15.5813	38.0684
Pb57	Tara Deep	Pale Beds	18.2158	15.5802	38.0664
B1	Navan Main Orebody	2-1 Lens	18.2274	15.5789	38.0899
B2	Navan Main Orebody	2-2 Lens	18.2194	15.5784	38.0813
B3	Navan Main Orebody	2-5 Lens	18.2174	15.5794	38.0832
		Lisheen			
LK0400/205	Main zone	Waulsortian	18.1946	15.5936	38.0631
LK1884/232	Main zone	Waulsortian	18.1929	15.5945	38.0600
LK0046/189	Main zone	Waulsortian	18.1496	15.5858	38.0021
LK0100/144	Main zone	Waulsortian	18.1983	15.5957	38.0726
LK1035/157	Main zone	Waulsortian	18.1662	15.5878	38.0233
LK974/179	Main zone	Waulsortian	18.1986	15.5965	38.0758
LK0822/176	Main zone	Waulsortian	18.1981	15.5956	38.0708
LK0937/179	Main zone	Waulsortian	18.1932	15.5882	38.0542
LK0152/203	Main zone	Waulsortian	18.1975	15.5961	38.0662
LK0458/217	Main zone	Waulsortian	18.2155	15.5993	38.1026
LK0227/234	Main zone	Waulsortian	18.1950	15.5908	38.0589
LK1915/199	Main zone	Waulsortian	18.1960	15.5951	38.0640
LK0717/193	Derryville	Waulsortian	18.1606	15.5883	38.0164
LK0839/160	Derryville	Waulsortian	18.2095	15.5973	38.0889
LK0952/192	Derryville	Waulsortian	18.2108	15.6004	38.0854
LK1010/187	Derryville	Waulsortian	18.1472	15.5864	37.9979
LK0173/132	Derryville	Waulsortian	18.2003	15.5952	38.0729
LK0141/201	Derryville	Waulsortian	18.1937	15.5893	38.0530

Table A3. *Cont.*

Sample ID	Orebody	Unit	^{206}Pb/^{204}Pb	^{207}Pb/^{204}Pb	^{208}Pb/^{204}Pb
LK0640/184	Derryville	Waulsortian	18.1584	15.5870	38.0125
LK0896/116	Derryville	Waulsortian	18.2137	15.5986	38.0990
LK0735/155	Derryville	Waulsortian	18.1925	15.5924	38.0594
LK0568/183	Bog Zone	Waulsortian	18.2164	15.5994	38.1032
LK1784/116	Bog Zone	Waulsortian	18.2085	15.5989	38.0939
LK1816/109	Bog Zone	Waulsortian	18.2093	15.5990	38.0955
LK1612/151	Bog Zone	Waulsortian	18.2075	15.6005	38.0834
LK1628/189	Bog Zone	Waulsortian	18.2053	15.5998	38.0834
LK0736/131	Bog Zone	Waulsortian	18.2057	15.5984	38.0824
ALD037	Island Pod	Waulsortian	18.1904	15.5915	38.0549
ALD015	Island Pod	Waulsortian	18.1917	15.5942	38.0584
ALD081	Island Pod	Waulsortian	18.1928	15.5921	38.0571
ALD050	Island Pod	Waulsortian	18.1931	15.5924	38.0551
ALD116	Island Pod	Waulsortian	18.1934	15.5937	38.0619
ALD068	Island Pod	Waulsortian	18.1940	15.5933	38.0590
ALD013	Island Pod	Waulsortian	18.1945	15.5932	38.0581
ALD088	Island Pod	Waulsortian	18.1945	15.5939	38.0593
ALD045	Island Pod	Waulsortian	18.1951	15.5944	38.0619

References

1. Wilkinson, J.J.; Hitzman, M.W. The Irish Zn–Pb Orefield: The View from 2014. In *Current Perspectives on Zinc Deposits*; Archibold, S.M., Piercey, S.J., Eds.; Irish Association for Economic Geology: Dublin, Ireland, 2015; pp. 59–72.
2. Derry, D.R.; Clark, G.R.; Gillatt, N. The Northgate base-metal deposit at Tynagh, County Galway, Ireland. *Econ. Geol.* **1965**, *60*, 1218–1237. [CrossRef]
3. Leeder, M.R. Upper Palaeozoic basins of the British Isles—Caledonide inheritance versus Hercynian plate margin processes. *J. Geol. Soc. Lond.* **1982**, *139*, 479–491. [CrossRef]
4. Monteiro, L.V.S.; Bettencourt, J.S.; Juliani, C.; de Oliveira, T.F. Geology, petrography, and mineral chemistry of the Vazante non-sulfide and Ambrośia and Fagundes sulfide-rich carbonate-hosted Zn–(Pb) deposits, Minas Gerais, Brazil. *Ore Geol. Rev.* **2006**, *28*, 201–234. [CrossRef]
5. Rajabi, A.; Rastad, E.; Canet, C. Metallogeny of Cretaceous carbonate-hosted Zn–Pb deposits of Iran: Geotectonic setting and data integration for future mineral exploration. *Int. Geol. Rev.* **2012**, *54*, 1649–1672. [CrossRef]
6. Andrew, C.J. The tectono-stratigraphic controls to mineralization in the Silvermines area, County Tipperary, Ireland. In *Geology and Genesis of Mineral Deposits in Ireland*; Andrew, C.J., Crowe, R.W.A., Finlay, S., Pennell, W.M., Pyne, J.F., Eds.; Irish Association for Economic Geology: Dublin, Ireland, 1986; pp. 377–417.
7. Ashton, J.H.; Downing, D.T.; Finlay, S. The geology of the Navan Zn–Pb orebody. In *Geology and genesis of mineral deposits in Ireland*; Andrew, C.J., Crowe, R.W.A., Finlay, S., Pennell, W.M., Pyne, J.F., Eds.; Irish Association for Economic Geology: Dublin, Ireland, 1986; pp. 243–280.
8. Boyce, A.J.; Stephen Little, C.; Russell, M. A New Fossil Vent Biota in the Ballynoe Barite Deposit, Silvermines, Ireland: Evidence for Intracratonic Sea-Floor Hydrothermal Activity About 352 Ma. *Econ. Geol.* **2003**, *98*, 649–656. [CrossRef]
9. Anderson, I.K.; Ashton, J.H.; Boyce, A.J.; Fallick, A.E.; Russell, M.J. Ore depositional processes in the Navan Zn–Pb deposit, Ireland. *Econ. Geol.* **1998**, *93*, 535–563. [CrossRef]
10. Hitzman, M.W.; Redmond, P.B.; Beaty, D.W. The carbonate-hosted Lisheen Zn–Pb-Ag deposits, County Tipperary, Ireland. *Econ. Geol.* **2002**, *97*, 1627–1655. [CrossRef]
11. Ashton, J.H.; Blakeman, R.J.; Geraghty, J.F.; Beach, A.; Coller, D.; Philcox, M.E. The Giant Navan carbonate-hosted Zn–Pb deposit—A review. In *Current Perspectives on Zinc Deposits*; Archibald, S.M., Piercey, S.J., Eds.; Irish Association for Economic Geology: Dublin, Ireland, 2015; pp. 85–122.
12. Wilkinson, J.J.; Eyre, S.L.; Boyce, A.J. Ore-forming processes in Irish-type carbonate-hosted Zn–Pb deposits: Evidence from mineralogy, chemistry, and isotopic composition of sulfides at the Lisheen mine. *Econ. Geol.* **2005**, *100*, 63–86. [CrossRef]

13. Ashton, J.H.; Beach, I.A.; Blakeman, R.J.; Coller, D.; Henry, P.; Lee, R.; Hitzman, M.; Hope, C.; Huleatt-James, S.; O'Donovan, B.; et al. *Discovery of the Tara Deep Zn–Pb Mineralization at the Boliden Tara Mine, Navan*; Success with Modem Seismic Surveys; SEG Special Publications; Society of Economic Geologists: Littleton, CO, USA, 2018; pp. 365–381.

14. Ashton, J.H. *Boliden Summary Report Resources and Reserves, Tara Mines*; Boliden: Stockholm, Sweden, 2018.

15. Ashton, J.H.; Black, A.; Geraghty, J.; Holdstock, M.; Hyland, E. The geological setting and metal distribution patterns of Zn + Pb + Fe mineralization in the Navan Boulder Conglomerate. In *The Irish Minerals Industry 1980–1990*; Bowden, A.A., Earls, G., O'Connor, P.G., Pyne, J.F., Eds.; Irish Association for Economic Geology: Dublin, Ireland, 1992; pp. 171–210.

16. Ashton, J.H.; Geraghty, J.F.; Holdstock, M.P.; O'Keeffe, W.G.; Martinez, N.; Peace, W.; Philcox, M.E. The Navan orebody-discovery and geology of the South West extension. In *Europe 's Major Base Metal Deposits*; Fusciardi, L., Earls, G., Stanley, G., Kelly, J.G., Ashton, J.H., Boland, M.B., Andrew, C.J., Eds.; Irish Association for Economic Geology: Dublin, Ireland, 2003; pp. 405–430.

17. Fallick, A.E.; Ashton, J.H.; Boyce, A.J.; Ellam, R.M.; Russell, M.J. Bacteria were responsible for the magnitude of the world-class hydrothermal base-metal orebody at Navan, Ireland. *Econ. Geol.* **2001**, *96*, 885–890. [CrossRef]

18. Blakeman, R.J.; Ashton, J.H.; Boyce, A.J.; Fallick, A.E.; Russell, M.J. Tirning of interplay between hydrothermal and surface fluids in the Navan Zn+Pb orebody, lreland: Evidence from metal distribution trends, mineral textures and d34S analyses. *Econ. Geol.* **2002**, *97*, 73–91. [CrossRef]

19. Gagnevin, D.; Boyce, A.J.; Barrie, C.D.; Menuge, J.F.; Blakeman, R.J. Zn, Fe and S isotope fractionation in a large hydrothermal system. *Geochim. et Cosmochim. Acta* **2012**, *88*, 183–198. [CrossRef]

20. Fusciardi, L.P.; Guven, J.F.; Stewart, D.R.A.; Carboni, V.; Walsh, J.J. The geology and genesis of the Lisheen Zn–Pb deposit, Co. Tipperary, Ireland. In *Europe's Major Base Metal Deposits*; Kelly, J.G., Andrew, C.J., Ashton, J.H., Boland, M.B., Earls, G., Fusciardi, L., Stanley, G., Eds.; Irish Association for Economic Geology: Dublin, Ireland, 2003; pp. 455–481.

21. Hitzman, M.W.; O'Connor, P.; Shearley, E.; Schaffalitzky, C.; Beaty, D.W.; Allan, J.R.; Thompson, T. Discovery and geology of the Lisheen Zn–Pb-Ag prospect, Rathdowney Trend, Ireland. In *The Irish Minerals Industry 1980–1990*; Bowden, A., Earls, G., O'Connor, P., Pyne, J., Eds.; Irish Association for Economic Geology: Dublin, Ireland, 1992; pp. 227–246.

22. Earls, G. The Lisheen Zn–Pb deposit. *Min. Mag.* **1994**, *6*, 6–8.

23. Shearley, E.; Redmond, P.; Goodman, R.; King, M. Guide to the Lisheen Zn–Pb-deposit. In *Irish Carbonate-hosted Zn–Pb Deposits*; Anderson, K., Ashton, J., Earls, G., Hitzman, M., Tear, S., Eds.; Society of Economic Geologists Guidebook Series; Society of Economic Geologists: Littleton, CO, USA, 1995; Volume 21, pp. 123–138.

24. Wilkinson, J.J.; Everett, C.E.; Boyce, A.J.; Gleeson, S.A.; Rye, D.M. Intracratonic crustal seawater circulation and the genesis of subseafloor Zn–Pb mineralization in the Irish ore field. *Geology* **2005**, *33*, 805–808. [CrossRef]

25. Torremans, K.; Kyne, R.; Doyle, R.; Guven, J.F.; Walsh, J.J. Controls on Metal Distributions at the Lisheen and Silvermines Deposits: Insights into Fluid Flow Pathways in Irish-Type Zn–Pb Deposits. *Econ. Geol.* **2018**, *113*, 1455–1477. [CrossRef]

26. Philcox, M.E. *Lower Carboniferous Lithostratigraphy of the Irish Midlands*; Irish Association for Economic Geology: Dublin, Ireland, 1984; 89p.

27. Philips, W.E.A.; Sevastopulo, G.D. Stratigraphic and structural setting of Irish mineral deposits. In *Geology and Genesis of Mineral Deposits in Ireland*; Andrew, C.J., Crowe, R.W.A., Finlay, S., Pennell, W.M., Pyne, J.F., Eds.; Irish Association for Economic Geology: Dublin, Ireland, 1986; pp. 1–30.

28. Gagnevin, D.; Menuge, J.F.; Kronz, A.; Barrie, C.; Boyce, A.J. Minor Elements in Layered Sphalerite as a Record of Fluid Origin, Mixing, and Crystallization in the Navan Zn–Pb Ore Deposit, Ireland. *Econ. Geol.* **2014**, *109*, 1513–1528. [CrossRef]

29. Fritschle, T.; Daly, J.S.; McConnell, B.; Whitehouse, M.J.; Menuge, J.F.; Buhre, S.; Mertz-Kraus, R.; Döpke, D. Peri-Gondwanan Ordovician arc magmatism in southeastern Ireland and the Isle of Man: Constraints on the timing of Caledonian deformation in Ganderia. *Geol. Soc. Am. Bull.* **2018**, *130*, 1918–1939. [CrossRef]

30. Van den Berg, R.; Daly, J.S.; Salisbury, M.H. Seismic velocities of granulite-facies xenoliths from Central Ireland: Implications for lower crustal composition and anisotropy. *Tectonophysics* **2005**, *407*, 81–99. [CrossRef]

31. Pannalal, S.J.; Symons, D.T.A.; Sangster, D.F. Paleomagnetic evidence for an early Permian age of the Lisheen Zn–Pb deposit, Ireland. *Econ. Geol. Bull. Soc. Econ. Geol.* **2008**, *103*, 1641–1655. [CrossRef]

32. Pannalal, S.J.; Symons, D.T.A.; Sangster, D.F. Paleomagnetic evidence of a Variscan age for the epigenetic Galmoy zinc-lead deposit, Ireland. *Terra Nova* **2008**, *20*, 385–393. [CrossRef]

33. Symons, D.T.A.; Smethurst, M.T.; Ashton, J.H. Paleomagnetism of the Navan Zn–Pb deposit, Ireland. *Econ. Geol. Bull. Soc. Econ. Geol.* **2002**, *97*, 997–1012. [CrossRef]

34. Symons, D.T.A.; Pannalal, S.J.; Kawasaki, K.; Sangster, D.F.; Stanley, G.A. Paleomagnetic age of the Magcobar Ba deposit, Silvermines, Ireland. In *Mineral Exploration and Research: Digging Deeper*; Andrew, C.J., Ed.; Irish Association for Economic Geology: Dublin, Ireland, 2007; pp. 377–380.

35. Hnatyshin, D.; Creaser, R.A.; Wilkinson, J.J.; Gleeson, S.A. Re-Os dating of pyrite confirms an early diagenetic onset and extended duration of mineralization in the Irish Zn–Pb ore field. *Geology* **2015**, *43*, 143–146. [CrossRef]

36. Kelley, S.P.; Fallick, A.E. High-precision, spatially resolved analysis of δ34S in sulfides using a laser extraction technique. *Geochim. et Cosmochim. Acta* **1990**, *54*, 883–888. [CrossRef]

37. Hollis, S.P.; Menuge, J.F.; Doran, A.; Güven, J.; Dennis, A.; Wilkinson, J.J.; Boyce, A.J.; Marks, F. Clumped C-O isotope temperature constraints for carbonate precipitation associated with Irish-type Zn–Pb orebodies. *J. Trans. Inst. Min. Metall. Sect. B* **2017**, *126*, 64–65. [CrossRef]

38. Hollis, S.P.; Menuge, J.F.; Dennis, P.; Doran, A.L.; Marca, A.; Davidheiser-Kroll, B.; Wilkinson, J.J.; Turner, O.; Guven, J.; Boyce, A. Tracking fluid temperature and composition in the world class Irish Zn–Pb ore field using clumped isotopes. in prep.

39. Dennis, P.F.; Myhill, D.J.; Marca, A.; Kirk, R. Clumped isotope evidence for episodic, rapid flow of fluids in a mineralized fault system in the Peak District, UK. *Journal of the Geological Society London* 2018. [CrossRef]

40. Yuan, H.; Yuan, W.; Cheng, C.; Liang, P.; Liu, X.; Dai, M.; Bao, Z.; Zong, C.; Chen, K.; Lai, S. Evaluation of lead isotope compositions of NIST NBS 981 measured by thermal ionization mass spectrometer and multiple-collector inductively coupled plasma mass spectrometer. *Solid Earth Sci.* **2016**, *1*, 74–78.

41. Wilkinson, J.J.; Lee, M.J. Cementation, hydrothermal alteration, and Zn–Pb mineralization of carbonate breccias in the Irish Midlands: Textural evidence from the Cooleen Zone, near Silvermines, County Tipperary—A reply. *Econ. Geol.* **2003**, *98*, 194–198. [CrossRef]

42. Hitzman, M.W.; Allan, J.R.; Beaty, D.W. Regional dolomitization of the Waulsortian limestone in southeastern Ireland: Evidence of large-scale fluid flow driven by the Hercynian orogeny. *Geology* **1998**, *26*, 547–550. [CrossRef]

43. Wilkinson, J.J.; Earls, G. A high temperature hydrothermal origin for black dolomite matrix Breccias in the Irish Zn–Pb Orefield. *Miner. Mag.* **2000**, *64*, 1077–1096. [CrossRef]

44. Kyne, R.; Torremans, K.; Güven, J.; Doyle, R.; Walsh, J. 3-D modeling of the lisheen and silvermines deposits, County Tipperary, Ireland: insights into structural controls on the formation of Irish Zn-Pb deposits. *Econ. Geol.* **2019**, *114*, 93–116. [CrossRef]

45. Wilkinson, J.J.; Crowther, H.L.; Coles, B.J. Chemical mass transfer during hydrothermal alteration of carbonates: Controls of seafloor subsidence, sedimentation and Zn–Pb mineralization in the Irish Carboniferous. *Chem. Geol.* **2011**, *289*, 55–75. [CrossRef]

46. Doran, A.L.; Hollis, S.P.; Menuge, J.F.; Piercey, S.J.; Boyce, A.J.; Guven, J.; Turner, O. Mineralizing Processes in the High-Grade Island Pod Zn–Pb Orebody, Lisheen, Ireland: A petrographic and S-Pb isotopic. in prep.

47. Ford, C.V. The Integration of Petrologic and Isotopic Data from the Boulder Conglomerate to Determine the Age of the Navan Orebody, Ireland. Ph.D. Thesis, University of Glasgow, Glasgow, UK, 1996; 176p.

48. Braithwaite, C.J.R.; Rizzi, G. The geometry and petrogenesis of hydrothermal dolomites at Navan, Ireland. *Sedimentology* **1997**, *44*, 421–440. [CrossRef]

49. Pearce, W.M. Carbonate-Hosted Zn–Pb Mineralisation within the Upper Pale Beds at Navan, Ireland. Ph.D. Thesis, University of Melbourne, Melbourne, Australia, 1999; 284p.

50. Eyre, S.L. Geochemistry of Dolomitization and Zn–Pb Mineralization in the Rathdowney Trend, Ireland. Ph.D Thesis, University of London, London, UK, 1998; 414p.

51. Boast, A.M.; Swainbank, I.G.; Coleman, M.L.; Halls, C. Lead isotope variation in the Tynagh, Silvermines and Navan base-metal deposits, Ireland. *Trans. Inst. Min. Metall.* **1981**, *90*, 115–119.

52. Mills, H.; Halliday, A.N.; Ashton, J.H.; Anderson, I.K.; Russell, M.J. Origin of a giant orebody at Navan, Ireland. *Nature* **1987**, *327*, 223–226. [CrossRef]

53. Marks, F.R. Remote Detection of Irish-Type Orebodies: An Investigation of the Navan Halo. Ph.D. Thesis, University College Dublin, Dublin, Ireland, 2015; 210p.

54. Everett, C.E.; Rye, D.M.; Ellam, R.M. Source or sink? An assessment of the role of the Old Red Sandstone in the genesis of the Irish Zn–Pb deposits. *Econ. Geol.* **2003**, *98*, 31–50.

55. O'Keeffe, W.G. Age and postulated source rocks for mineralisation in central Ireland, as indicated by lead isotopes. In *Geology and Genesis of Mineral Deposits in Ireland*; Andrew, C.J., Crowe, R.W.A., Finlay, S., Pennell, W.M., Pyne, J.F., Eds.; Irish Association for Economic Geology: Dublin, Ireland, 1986; pp. 617–624.

56. Walshaw, R.D.; Menuge, J.F.; Tyrrell, S. Metal sources of the Navan carbonate-hosted base metal deposit, Ireland: Nd and Sr isotope evidence for deep hydrothermal convection. *Miner. Depos.* **2006**, *41*, 803–819. [CrossRef]

57. Bischoff, J.L.; Radtke, A.S.; Rosenbauer, R.J. Hydrothermal alteration of graywacke by brine and seawater: Roles of alteration and chloride complexing on metal solubilization at 200 °C and 350 °C. *Econ. Geol.* **1981**, *76*, 659–676. [CrossRef]

58. Wilkinson, J.J. A review of fluid inclusion constraints on mineralization in the Irish ore field and implications for the genesis of sediment-hosted Zn–Pb deposits. *Econ. Geol.* **2010**, *105*, 417–442. [CrossRef]

59. Russell, M.J. Extension and convection: A genetic model for the Irish Carboniferous base metal and barite deposits. In *Geology and Genesis of Mineral Deposits in Ireland*; Andrew, C.J., Crowe, R.W.A., Finlay, S., Pennell, W.M., Pyne, J.F., Eds.; Irish Association for Economic Geology: Dublin, Ireland, 1986; pp. 545–554.

60. Goodfellow, W.D.; Lydon, J.W. Sedimentary exhalative (SEDEX) deposits. In *Mineral Deposits of Canada: A Synthesis of Major Deposit Types, District Metallogeny, the Evolution of Geological Provinces, and Exploration Methods*; Goodfellow, W.D., Ed.; Special Publication No. 5; Geological Association of Canada, Mineral Deposits Division: St. John's, NL, Canada, 2007; pp. 163–183.

61. Banks, D.A.; Boyce, A.J.; Samson, I.M. Constraints on the origins of fluids forming Irish Zn–Pb–Ba deposits: Evidence from the composition of fluid inclusions. *Econ. Geol.* **2002**, *97*, 471–480. [CrossRef]

62. Machel, H.G.; Krouse, H.R.; Sassen, R. Products and distinguishing criteria of bacterial and thermochemical sulfate reduction. *Appl. Geochem.* **1995**, *10*, 373–389. [CrossRef]

63. Altinok, E. Zn–Pb–Fe Mineralization Process, Evolution of Sea Water Oxidation State in a Restricted Basin, and Diagenesis of Deep Water Calcareous Sediments: Geochemical and Geological Study of the Navan Deposit, Dublin Basin, Ireland. Ph.D. Thesis, Colorado School of Mines, Golden, CO, USA, 2005; 160p.

64. Large, R.R.; Halpin, J.A.; Danyushevsky, L.V.; Maslennikov, V.V.; Bull, S.W.; Long, J.A.; Gregory, D.D.; Lounejeva, E.; Lyons, T.W.; Sack, P.J. Trace element content of sedimentary pyrite as a new proxy for deep-time ocean–atmosphere evolution. *Earth Planet. Sci. Lett.* **2014**, *389*, 209–220. [CrossRef]